AFRL-RX-WP-TR-2018-0071

BURNER RIG TESTING OF A500® C/SiC

Larry P. Zawada
Universal Technology Corporation

Jennifer Pierce
UDRI

Craig Przybyla
AFRL/RXCCP

17 MARCH 2018
Final Report

AIR FORCE RESEARCH LABORATORY
MATERIALS AND MANUFACTURING DIRECTORATE
WRIGHT-PATTERSON AIR FORCE BASE, OH 45433-7750
AIR FORCE MATERIEL COMMAND
UNITED STATES AIR FORCE

NOTICE AND SIGNATURE PAGE

Using Government drawings, specifications, or other data included in this document for any purpose other than Government procurement does not in any way obligate the U.S. Government. The fact that the Government formulated or supplied the drawings, specifications, or other data does not license the holder or any other person or corporation; or convey any rights or permission to manufacture, use, or sell any patented invention that may relate to them.

This report was cleared for public release by the USAF 88th Air Base Wing (88 ABW) Public Affairs Office (PAO) and is available to the general public, including foreign nationals.

Qualified requestors may obtain copies of this report from the Defense Technical Information Center (DTIC) (http://www.dtic.mil).

AFRL-RX-WP-TR-2018-0071 HAS BEEN REVIEWED AND IS APPROVED FOR PUBLICATION IN ACCORDANCE WITH ASSIGNED DISTRIBUTION STATEMENT.

//Signature//
CRAIG P. PRZYBYLA
Project Engineer
Composite Branch
Structural Materials Division
Materials and Manufacturing Directorate

//Signature//
TIMOTHY D. BREITZMAN
Section Chief
Composite Branch
Structural Materials Division
Materials and Manufacturing Directorate

//Signature//
AMBER I. DAVIS
Deputy Division Chief
Structural Materials Division
Materials And Manufacturing Directorate

This report is published in the interest of scientific and technical information exchange, and its publication does not constitute the Government’s approval or disapproval of its ideas or findings.

REPORT DOCUMENTATION PAGE

Form Approved
OMB No. 0704-0188

1. REPORT DATE *(DD-MM-YY)*	2. REPORT TYPE	3. DATES COVERED *(From - To)*
17 March 2018	Final	1 January 2005 – 31 December 2007

4. TITLE AND SUBTITLE
BURNER RIG TESTING OF A500® C/SiC

5a. CONTRACT NUMBER
In-House

5b. GRANT NUMBER

5c. PROGRAM ELEMENT NUMBER
62102F

6. AUTHOR(S)
Larry P. Zawada –UTC
Jennifer Pierce – UDRI
Craig Przybyla – AFRL/RXCC

5d. PROJECT NUMBER
4347

5e. TASK NUMBER

5f. WORK UNIT NUMBER
X0S7

7. PERFORMING ORGANIZATION NAME(S) AND ADDRESS(ES)

AFRL/RXCC
Composites Branch; Structural Materials Division
Materials and Manufacturing Directorate
2230 Tenth Street, Suite 1
Wright Patterson Air Force Base, OH 45433

Universal Technology Corporation
1270 North Fairfield Road
Dayton, Ohio 45432-2600

University of Dayton Research Institute
Structural Integrity Division
300 College Park
Dayton, OH 45469-0128

8. PERFORMING ORGANIZATION REPORT NUMBER
AFRL-RX-WP-TR-2018-0071

9. SPONSORING/MONITORING AGENCY NAME(S) AND ADDRESS(ES)

Air Force Research Laboratory
Materials and Manufacturing Directorate
Wright-Patterson Air Force Base, OH 45433-7750
Air Force Materiel Command
United States Air Force

10. SPONSORING/MONITORING AGENCY ACRONYM(S)
AFRL/RXCC

11. SPONSORING/MONITORING AGENCY REPORT NUMBER(S)
AFRL-RX-WP-TR-2018-0071

12. DISTRIBUTION/AVAILABILITY STATEMENT
Distribution Statement A. Approved for public release; distribution unlimited

13. SUPPLEMENTARY NOTES:
PA Case Number: 88ABW-2018-0065; Clearance Date: 08 Jan 2018. This document contains color.

14. ABSTRACT (*Maximum 200 words*):
A dedicated experimental test program characterized the durability behavior of A500® C/SiC ceramic matrix composite material at room and elevated temperature. Specimens were exposed to salt fog and then burner rig thermal cycles. This report describes the conditioning and the residual tensile behavior after exposure.

15. SUBJECT TERMS
ceramic matrix composites, burner rig, salt fog exposure, C/SiC, sealing, glassy phases, creep, fatigue, tensile

16. SECURITY CLASSIFICATION OF:			17. LIMITATION OF ABSTRACT:	18. NUMBER OF PAGES	19a. NAME OF RESPONSIBLE PERSON (Monitor)
a. REPORT	b. ABSTRACT	c. THIS PAGE			Craig Przybyla
Unclassified	Unclassified	Unclassified	SAR	74	19b. TELEPHONE NUMBER *(Include Area Code)* (937) 255-9396

TABLE OF CONTENTS

Section **Page**

LIST OF FIGURES

Figure **Page**

LIST OF TABLES

Table **Page**

1.0 SUMMARY

This report describes results from a burner rig test evaluation of SEPCARBINOX® A500, which is an advanced ceramic-matrix composite (CMC) material system made from carbon fiber-reinforced silicon carbide (C/SiC) manufactured by Snecma Propulsion Solide (SPS). The matrix is unique in that it is made up of sequential layers containing silicon (Si), carbon (C), and boron (B). The layering is intentionally used for two reasons. The first is that the layers are both hard and soft;, thus, providing a crack-blunting mechanism, which keeps cracks from penetrating directly into the interior of the CMC. Secondly, the boron-containing layers form glassy phases which protect the matrix, fibers, and fiber interface coating from attack in aggressive oxidizing environments.

The historical solution for protecting the matrix and fibers in C/SiC materials is through exterior environmental barrier coatings (EBC). However, EBCs add to the complexity and cost of component manufacture, and leave the material's performance dependent upon the durability of the coatings. In addition, the CMC and coatings tend to have coefficient of thermal expansion (CTE) mismatch issues, which often result in the EBC coating spalling off the CMC. The novel approach that SPS has taken provides protection on the surface and throughout the entire composite by means of "self-healing" mechanisms contained within the ceramic matrix, which eliminate the need for additional exterior EBCs.

The burner rig evaluation described in this report is an effort by the United States Air Force (USAF) to simulate, in a laboratory environment, the service conditions the A500 C/SiC CMC would experience in turbine engine exhaust applications. To this end, the testing combined the aggressive environmental conditions of cyclic hot gas flow coupled with intermittent salt fog exposure (consistent with what a turbine engine exhaust nozzle would experience when operated near a marine environment) to evaluate A500's performance by documenting its retained tensile properties.

The results presented in this report include an assessment of the material condition and the retained tensile properties of the burner rig-exposed coupons compared to as-manufactured material.

2.0 INTRODUCTION

2.1 Background

There is growing interest in developing, testing, and deploying CMCs into commercial and military aerospace gas turbine engines due to their durability under extreme conditions and weight-savings potential. For military applications, the focus is on the afterburning section of the turbine engine, including the flameholder, augmentor liner, and both the convergent and divergent segments of the exhaust nozzle. These are demanding applications because of the high temperatures and rapid thermal cycles.

Each year, a large number of exhaust nozzle divergent flaps and seals are replaced before reaching their scheduled life, causing a large maintenance burden. Engineering evaluation and lab testing have shown that premature distress of divergent seals is due to severe environmental exposure, including: high-temperature-induced creep deformation, rapid thermal cycles, severe thermal gradients, and high acoustic loading.

CMCs are being evaluated to replace traditional nickel-based superalloys because they offer high-temperature capability, limited or no property debit with temperature, have a density that is a third of that of the nickel-based superalloy, and do not require cooling air [1]. CMCs being considered for gas turbine applications cover a wide range of fibers and matrices, and are fabricated by chemical-vapor infiltration (CVI), sol-gel techniques, polymer infiltration and pyrolysis (PIP), and melt infiltration (MI) [2,3]. For exhaust nozzle divergent flaps and seals, there is a large body of work that was performed on CVI- and PIP-processed CMC materials. It was in 1997 that the United States Navy (USN) approved full production qualification of SiC/C CMC divergent flaps and seals for the F414 engine that powers the F-18-E/F Super Hornet. [4,5]. Other investigators have looked at CVI material systems as part of nozzle flap and seal applications [6,7].

A CMC system developed by SPS was evaluated for a divergent seal application. This material is SEPCARBINOX® A500, a C/SiC composite with a 3-D weave configuration for improved delamination resistance [8-12] and a sequenced CVI matrix that is self-sealing for protection of the carbon fibers.

Material acceptance testing at the coupon level had already been completed and reported [9-12]. A database of 65 coupons from nine production runs of A500 showed that the material consistently exceeded the acceptance criteria for ultimate tensile strength (UTS) for the application. The UTS of the material in the database is 252 ± 25 MPa, compared to the acceptance level UTS of 170 MPa. The final stage of testing involved what the industry calls “killer tests” – a series of tests involving aggressive environmental conditions. The aim was to identify and expose any material weaknesses prior to proceeding to ground testing and insertion into actual fielded applications. Such tests were performed on material coupons and reported elsewhere [13]. This earlier testing involved a combination of two-hour dwell fatigue testing in both air and steam environments. Results showed that the A500 CMC consistently performed better than other C/SiC CMC systems.

As part of the effort to expand the aggressive evaluation of the A500 material, burner rig tests were undertaken at the USN test facility at Naval Air Systems Command (NAVAIR). Burner rig testing simulates the in-flight condition of applying an afterburner, as used on military aircraft engines for takeoff and reaching high-speed supersonic flight. The lighting of an afterburner results in a very rapid thermal spike of the exhaust nozzle hardware. The longer the afterburner is operated, the higher the temperature rises. In addition, aircraft are often operated near a marine saltwater environment. Therefore, in addition to the burner rig exposures, the test specimens were exposed to salt fog before and between intervals of burner rig testing. Furthermore, some specimens were creep tested and others fatigue tested prior to the salt fog and burner rig exposure with the intention of "pre-conditioning" them by exposing them beyond the predicted in-flight mechanical loads in order to introduce additional matrix cracks. This report focuses on the results of the expanded laboratory "killer testing" involving burner rig and salt fog testing.

2.2 Program Objectives

The objective of this research was to determine the retained tensile properties of a state-of-the-art ceramic matrix composite system exposed to burner rig plus salt fog environmental conditions.

3.0 PROCEDURES

3.1 Materials Description

As mentioned, SEPCARBINOX® A500 is a C/SiC composite – carbon fibers are reinforced by a SiC matrix. The reinforcement is T300 (3000 fibers per tow) Toray carbon-fiber fabric preforms consolidated with layers of materials that include silicon carbide. Fabrication of this material requires two main steps.

The first step in manufacturing this material is the preparation of the fiber preform. A ply-to-ply angle interlock is used to reduce delamination sensitivity that is common for 2-D CMC materials [8] and to minimize the loss of in-plane properties associated with many through-thickness orthogonal 3-D weaves. The number of reinforced layers is adjustable in order to obtain the appropriate composite thickness (typically between 2 mm and 7 mm). The number of layers for this evaluation was chosen to obtain a composite thickness of 4 mm before the start of the CVI process. These reinforcements have been optimized to obtain orthotropic composites, with in-plane mechanical characteristics close to a 2-D material. A illustration of a typical ply-to-ply angle interlock weave is shown in Figure 1.

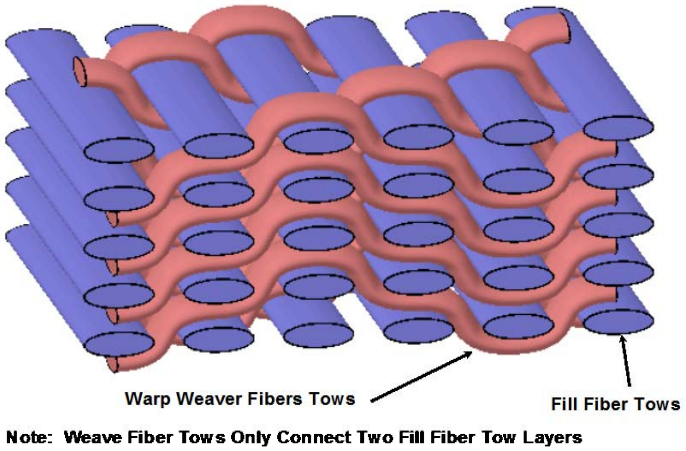

Figure 1. Illustration of a Ply-to-Ply Angled Interlock Weave

The second fabrication step involves formation of the ceramic matrix by CVI. A novel matrix technology that combines sequential layers of carbides deposited by the CVI process with specific sequences of Silicon (Si), Carbon (C), and Boron (B) has been developed and applied to the A500 composite [8] for temperature durability up to 1200ºC. The sequential layers that make up the matrix consist of flexible layers and relatively rigid ceramic layers. The flexible layers can consist of pyrolytic carbon, boron nitride, boron-doped carbon, and others that form self-healing phases when oxidized. The flexible layers represent 4% to 20% of the total thickness of the layers that form the sequenced matrix. The rigid ceramic layers form a portion of the matrix and are made from carbides, borides, and silicides, including boron carbide ($B_{12}C_2$ and SiC). The matrix is essentially comprised of two successive sequences of BC/$B_{13}C_2$ and BC/SiC. Figure 2 is a low-magnification micrograph of a polished cross-section of the A500 CMC which shows how the fiber tows weave up into the ply above and then down into the ply below. Large

pockets of porosity can be observed between the fiber tows, and much finer porosity is observed within the fiber tows. During the CVI process, the individual layers within the matrix are kept very small. Then, during the final stages of processing, the conditions are changed and much larger layers are deposited on the surface of the CMC. This thicker layered structure on the surface of the fiber preform is not a coating, but simply an extension of the layered matrix. The as-produced test specimens had a fiber volume fraction of 43%, a density of 2.03 g/cm^3, and porosity on the order of 12% to 14%.

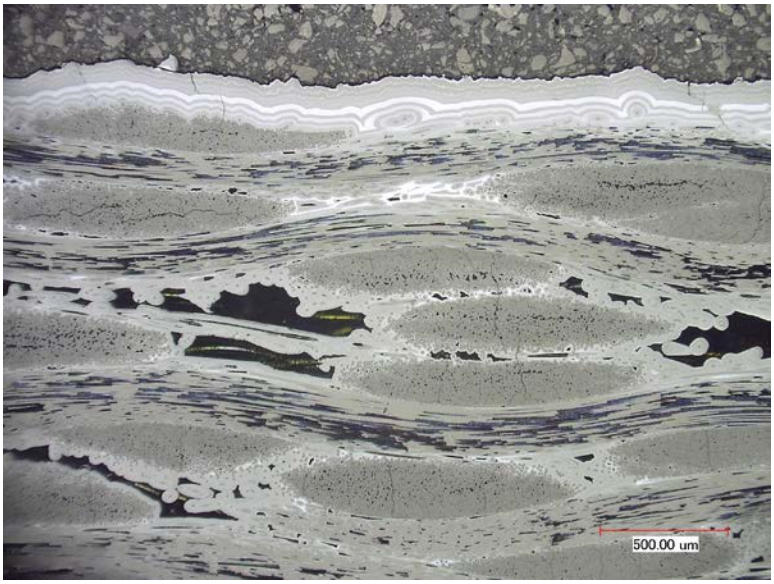

Figure 2. Optical micrograph of A500 C/SiC Cross-Section Illustrating Its Layered Nature

A key feature of the composite is the ability for the layered ceramic matrix and the outer surface to seal itself if damaged. This characteristic eliminates the need for an additional exterior barrier coating [8]. The principle of the self-sealing approach in the design of this matrix is that, when a crack forms in the ceramic matrix, one of the layers would react with incoming oxygen; the product of this reaction is a glassy phase that expands and acts to seal off the matrix crack and prevent oxidation of the carbon fibers. The more rigid SiC layers act to form multiple barriers preventing all of the sealing phases from reacting all at once – only one layer at a time. A high-magnification scanning electron microscope (SEM) micrograph illustrating the glassy-phase formation of the matrix to fill matrix cracks is shown in Figure 3. In addition to the self-sealing mechanism, the sequenced matrix and outer layers are very effective at deflecting and bifurcating cracks. The images in Figure 4 and Figure 5 illustrate an example of crack deflection and branching due to sequencing in the ceramic matrix on the outer surface. Standard C/SiC made by CVI experiences very large cracks that are often many microns in width and occur both at the surface and in the interior of the CMC. However, with A500, the deflections of the matrix cracks result in much smaller crack mouth opening displacements (CMOD), allowing for easier sealing of the cracks.

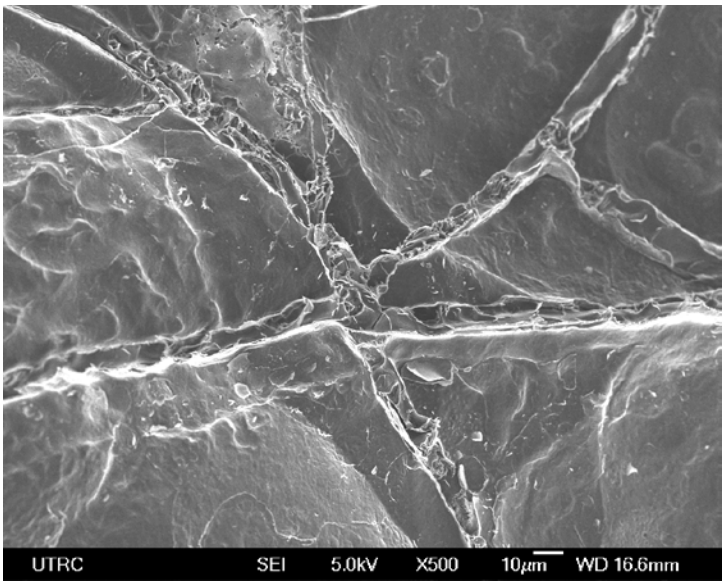

Figure 3. SEM Image Illustrating Matrix Glass Formation that Occurs in A500 C/SiC

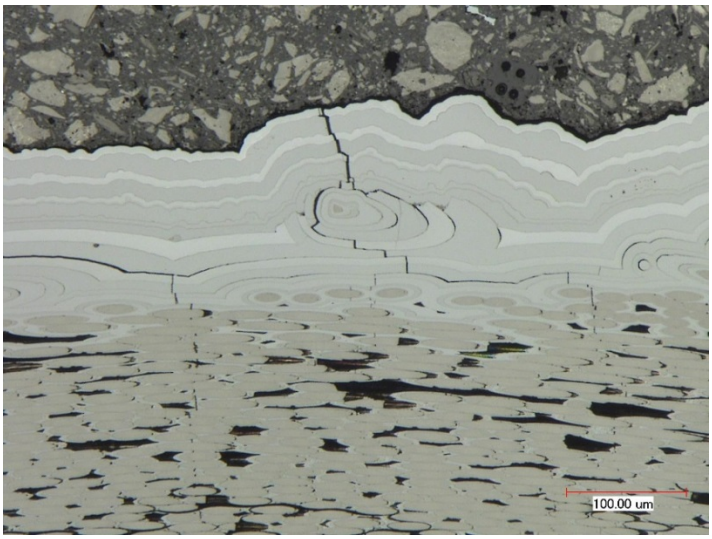

Figure 4. Optical Micrograph of A500 C/SiC Depicting Crack Deflection Due to Layers in the Material

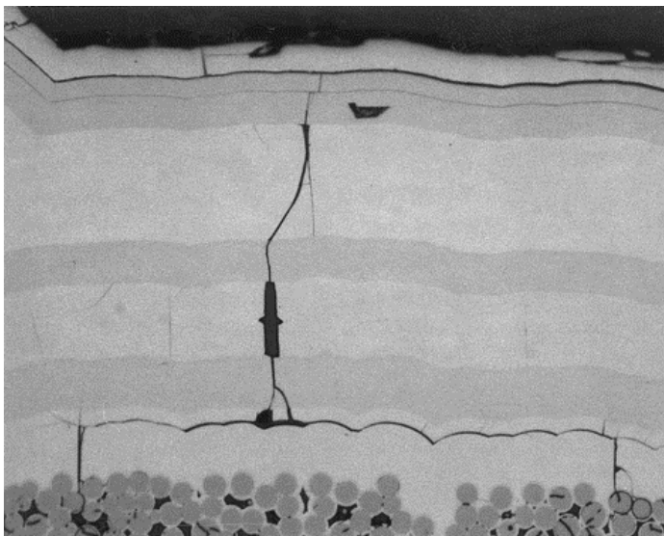

Figure 5. Optical Micrograph of A500 C/SiC Depicting Crack Deflection Due to Layers in the Material

A typical-room temperature tensile stress-versus-strain trace for A500 C/SiC is shown in Figure 6. The calculation of efficient strength will be described in a following section. It is important to note that, since there are carbon fibers in a SiC matrix, the CTE difference between the fibers and matrix results in extensive matrix cracks during processing. Therefore, during a tension test, there is usually only a short initial linear region followed by a gradual transition to non-linear stress-versus-strain behavior. This transition typically occurs between 30 MPa and 70 MPa for as-manufactured material. After the proportional limit is reached, there is extensive non-linear behavior up to approximately 150 MPa, and then the traces appear to be fairly linear up to near the UTS. It is suggested that, in this region, the CMC is completely micro-cracked and most of the load is being carried by the fibers. Stiffness is approximately 125 GPa and UTS is around 300 MPa. The A500 CMC exhibits good composite behavior and strain to failure typically exceeds 0.5%.

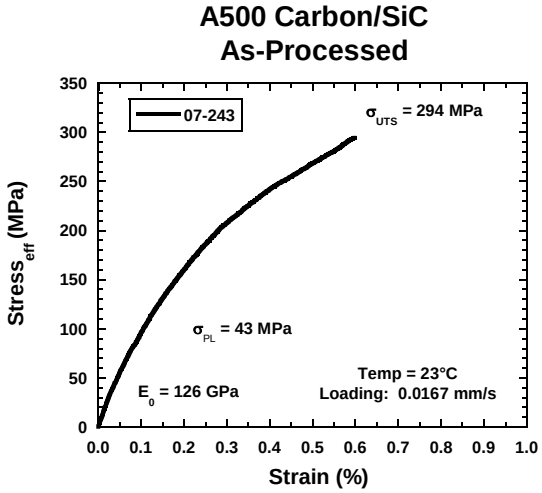

Figure 6. Typical Room-Temperature Tensile Stress-Versus-Strain Trace for As-Manufactured A500 C/SiC

3.2 Test Material

SPS manufactured four plates of A500 for this testing program which produced a total of 68 test coupons. A designated number of the coupons went to NAVAIR for the burner rig test matrix and the others were retained by SPS for material lot acceptance testing and pre-conditioning test parameter definition. The following describes the test coupons and the results from the materials acceptance testing performed by SPS.

The four manufactured plates were 200 mm × 200 mm (7.8" × 7.8") with reference numbers 432, 433, 434, and 435 that were processed by interphase deposition and hardening, a first CVI cycle, coupon machining, and a second CVI cycle. Physical properties of the four plates are reported in Table 1 where the hardening thickness refers to the material thickness without the seal coat. This dimension is used for the thickness when calculating the strength of the tensile coupons. The assumption is that the external seal-coat layer is significantly micro-cracked and does not provide any structural load-carrying capability. Use of a hardening thickness allows for a more accurate comparison between A500 materials with different thicknesses. Final densities listed in the table are higher than the minimum criteria of d > 1.90 g/cc.

Table 1. Physical Properties of Plates Used for Test Specimens

Plate ID	Preform I.D.	Hardening Thickness (mm)	Fiber Volume Ration (%)	Final Density (g/cc)	Porosity (%)
#432	2291689	2.6	43.5	2.03	8.7
#433				2.03	7.7
#434				2.06	7.5
#435				2.06	8.5

3.3 Specimen Geometry

A dogbone specimen geometry was selected for all tensile and durability testing. SPS had used a much larger test specimen design for generation of their data base. However, they were too large to be tested in the NAVAIR burner rig, so a smaller overall specimen length of 150 mm (6″) was selected, as this is the maximum length the rig could accommodate. A 28 mm (1.1″) straight section was selected to accommodate high-temperature extensometers with ceramic extension rods that typically have either a 12.5 mm (0.5″) or 25 mm (1″) gage length. In addition, several straight-sided specimens were manufactured which were used as set-up coupons and for calibration runs of the burner rig. Schematic diagrams of the two specimen geometries used for the burner rig and salt fog exposures are shown in Figure 7.

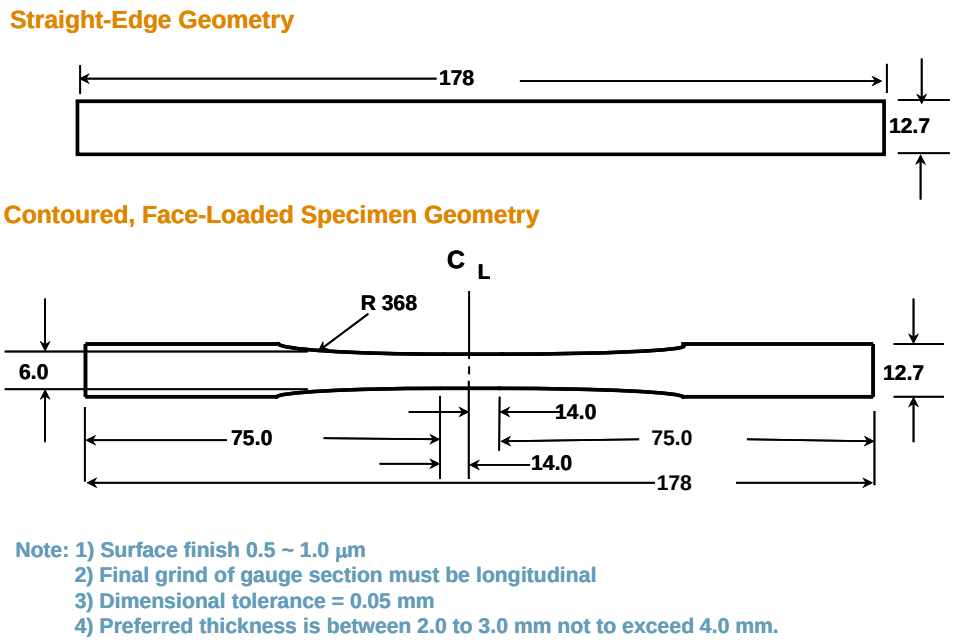

Figure 7. Drawings Of The Straight-Edge and Dogbone Specimens Used for Burner Rig Setup Trials and Testing

Several other test specimens were also machined from the panels. First, one extra-large dogbone specimen was machined from each panel, which is the original test specimen design used by SPS to develop the A500 CMC and subsequent database. The specimen design shown in Figure 7 had never been used by SPS and there was some concern that, given the unique weave used to make the fiber preform, the test results for the much smaller specimen might not accurately measure strength. Therefore, tensile strength information in the database developed by SPS from the original large specimens was used to directly compare to the results generated in this study on the smaller specimens. In addition, three dogbone specimens were machined out in the 90°, or "2" direction, of the panel that were used to determine if there was a difference in tensile strength between the 0°, or "`1" direction, and the 90° direction. A diagram illustrating how each of the 17 specimens were machined from each of the four plates is shown in Figure 8. A total of 13 test specimens were used for acceptance testing, while 36 dogbone and 12 straight-edge coupons were designated for the burner rig testing. All of the remaining test specimens were held in reserve.

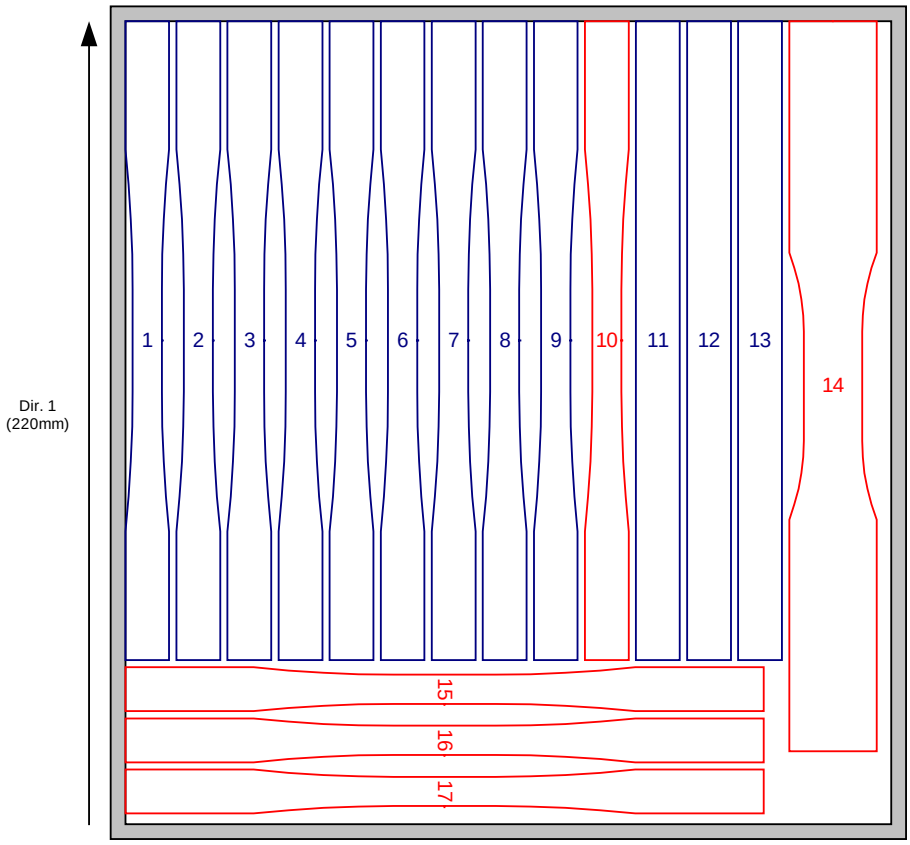

Figure 8. Cutting Diagram of Plates #432 to #435.
Coupons Designated for Burner Rig Testing in Black and for SPS in Red.

Some of the specimens from each plate were retained by SPS for acceptance testing. Those included the comparatively large face-loaded dogbone specimen, one of the standard-sized dogbones in the "1" (axial) direction, and the standard-sized dogbone specimens oriented in the "2" (transverse) direction from each plate. A summary of the test coupons from the four plates and their test designations is shown in Table 2.

Table 2. Test Coupon Designations From Four Plates of A500

Total Number of Specimens	Direction	SPS ID	Geometry	Test
36	"1" (axial)	1-9	Dogbone	NAVAIR Burner Rig Test
4	"1" (axial)	10	Dogbone	SPS Acceptance Test
12	"1" (axial)	11-13	Straight Edge	NAVAIR Test
4	"1" (axial)	14	Large Dogbone	SPS Acceptance Test
12	"2" (transverse)	15-17	Dogbone	SPS Acceptance Test

The 36 dogbone coupons designated for burner rig testing were given new consecutive identification numbers to provide for a unique reference regardless of the plate of origin. SPS had numbered the specimens as 1 through 17 in each plate, according to their location. Table 3 lists the 36 burner rig test coupons and their plates of origin to establish a correlation between the original SPS identification number and the NAVAIR burner rig test identification number.

Table 3. Test Coupon Designations from Four plates of A500

	Coupon ID Number	
Plate of Origin	**SPS**	**NAVAIR**
#432	1	7
	2	10
	3	16
	4	1
	5	25
	6	4
	7	13
	8	22
	9	19
#433	1	9
	2	8
	3	28
	4	34
	5	26
	6	31
	7	17
	8	14
	9	12
#434	1	11
	2	20
	3	29
	4	35
	5	27
	6	32
	7	5
	8	2
	9	23
#435	1	21
	2	15
	3	30
	4	36
	5	6
	6	33
	7	3
	8	18
	9	24

3.4 Test Plan

The test matrix for this program was divided into three main sets of tests: The first involved tensile acceptance and verification testing of as-manufactured material. These results would be compared to the extensive SPS database and serve as a baseline for all subsequent experiments. The second set of experiments involved the burner rig plus salt fog exposure. The third set involved pre-conditioning specimens using fatigue or creep, and then subjecting them to the burner rig plus salt fog exposure. SPS reports that the maximum-use temperature of the A500 material is approximately 1100°C, and this was selected as the maximum temperature for the burner rig testing.

3.4.1 Acceptance Tension Testing.

Acceptance testing was required to verify the manufacturing process, and SPS conducted tension tests on the machined specimens from each panel to verify the mechanical properties fell within the established A500 database. They tested one in both the 0° ("1") orientation and one in the 90° ("2") direction, as well as the larger dogbone specimens. The USAF conducted tension tests on samples 25, 26, and 27. Results from the seven tensile tests on the as-manufactured material which provided a baseline comparison to the tensile results generated on the coupons tested in the burner rig.

3.4.2 Burner Rig Plus Salt Fog.

Since the main goal of this project was to determine if the A500 C/SiC CMC could perform well in an aerospace turbine engine afterburner plus marine environment, burner rig plus salt fog exposure experiments were conducted. The burner rig carousel could hold up to 12 specimens at a time. For the first run, four different levels of exposure were tested, as illustrated by the schematic in Figure 9. The salt fog exposure was performed prior to burner rig testing and then after every 300 burner rig cycles. The "×2", "×3", and "×4" on the schematic indicate the number of times the sequence shown was repeated. The total number of burner rig cycles tested was 300, 600, 900, and 1200. The corresponding amounts of salt fog exposures were 24, 48, 72, and 96 hours, respectively. A total of 12 exposure tests were performed, after which, the specimens were tension tested by the USAF. The specimen numbers were as follows. For 300 burner rig cycles the specimens were #1, 2, 3. For 600 burner rig cycles the specimens were #13, 14, 15. For 900 burner rig cycles the specimens were #4, 5, 6. For 1200 burner rig cycles the specimens were #16, 17, 18.

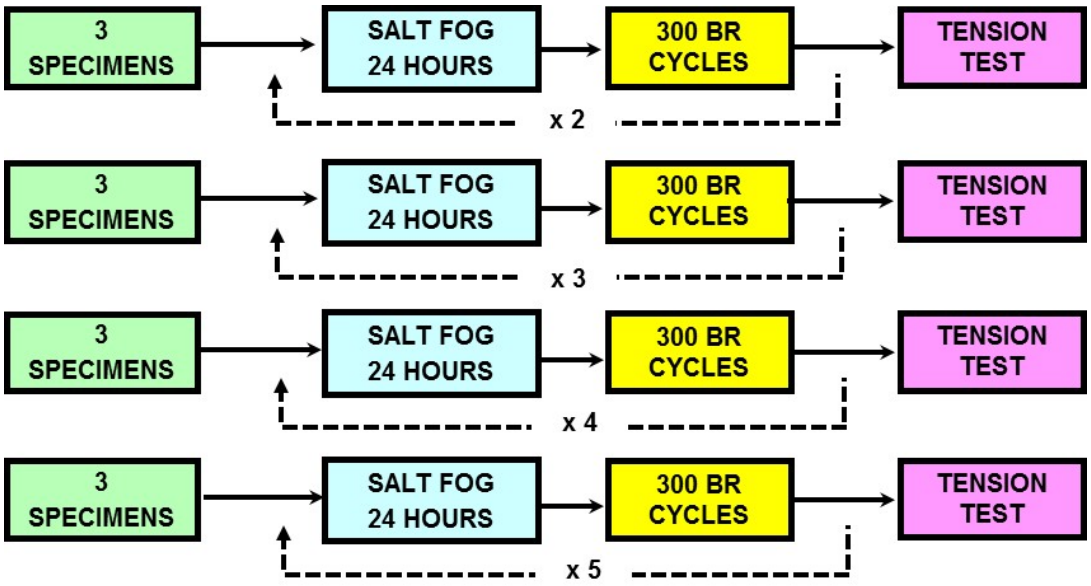

Figure 9. Schematic representation of the Test Matrix Addressing Burner Rig Plus Salt Fog Exposure Cycles

3.4.3 Creep and Fatigue Pre-conditioning Plus Burner Rig Plus Salt Fog.

This portion of the test matrix evaluated the effects of pre-conditioning prior to salt fog and burner rig exposure. As the schematic in Figure 10 shows, three specimens saw only 1500 burner rig cycles. The remaining nine test specimens were periodically exposed to salt fog. The salt fog exposure was performed prior to the start of burner rig testing, as well as after every 300 burner rig cycles. The "x 5" symbol and the loop drawn are to indicate that the sequence was repeated 5 times for a total of 1500 burner rig cycles. Each salt fog exposure was for 24 hours, for a total salt fog exposure of 120 hours for each specimen.

Three specimens saw 1500 cycles of burner rig plus salt fog and saw no pre-conditioning. The six remaining specimens were pre-conditioned, either by creep or fatigue, prior to the first salt fog exposure. Three specimens saw creep conditioning plus the burner rig plus salt fog, while three specimens saw fatigue conditioning followed by burner rig plus salt fog. The objective of pre-conditioning was to impart additional matrix cracking in the A500 C/SiC CMC that would potentially provide additional pathways for environment to ingress, thus testing any limitations of the "self-healing" mechanisms in the material.

NAVAIR tension tested the three specimens that only saw 1500 burner rig cycles (specimens # 10, 11, 12). Pratt & Whitney tension tested the three specimens that saw 1500 burner rig cycles plus 120 hours salt fog exposure (specimens7, 8, 9), as well as the creep pre-conditioned specimens (specimens #28, 29, 30) and the fatigue pre-conditioned specimens (specimens #31, 32, 33).

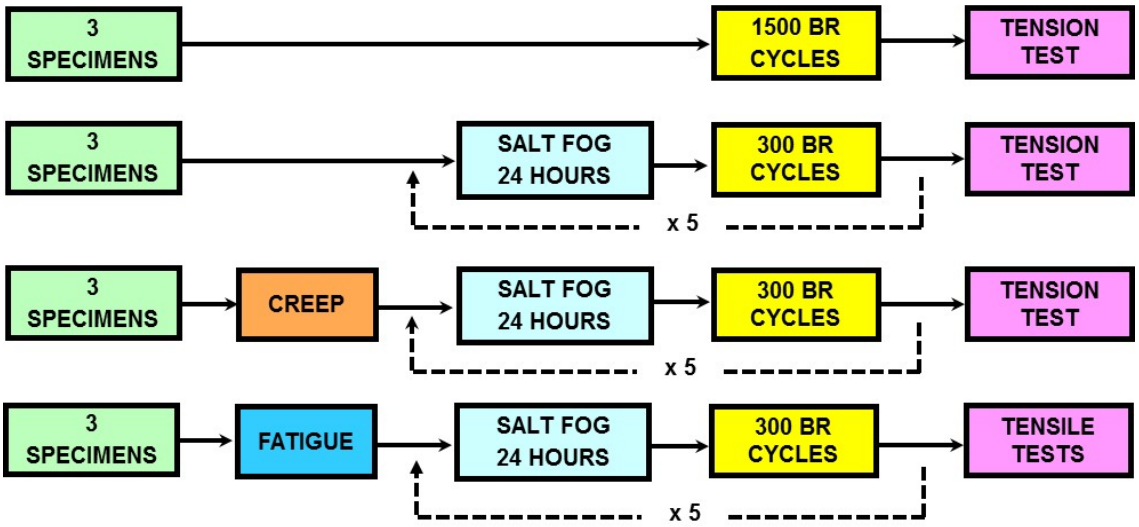

Figure 10. Schematic Representation Of The Test Matrix Addressing Pre-conditioned Specimens Plus Burner Rig Plus Salt Fog

3.4.4 Pre-conditioning: Determination of Test Parameters

SPS demonstrated test parameters in creep at an efficient strength level of 90 MPa and temperatures of 1200°C (acceptance test specimen #435-14), and in fatigue at 90 MPa and 600°C (acceptance test specimen #433-14). Both tests were stopped at 167 hours, without failure, in accordance with a minimum time criteria of 150 hours. The resulting displacement-versus-time traces for both tests are shown in Figure 11. The measured displacements were small and both specimens ran out past the life criterial of 150 hours.

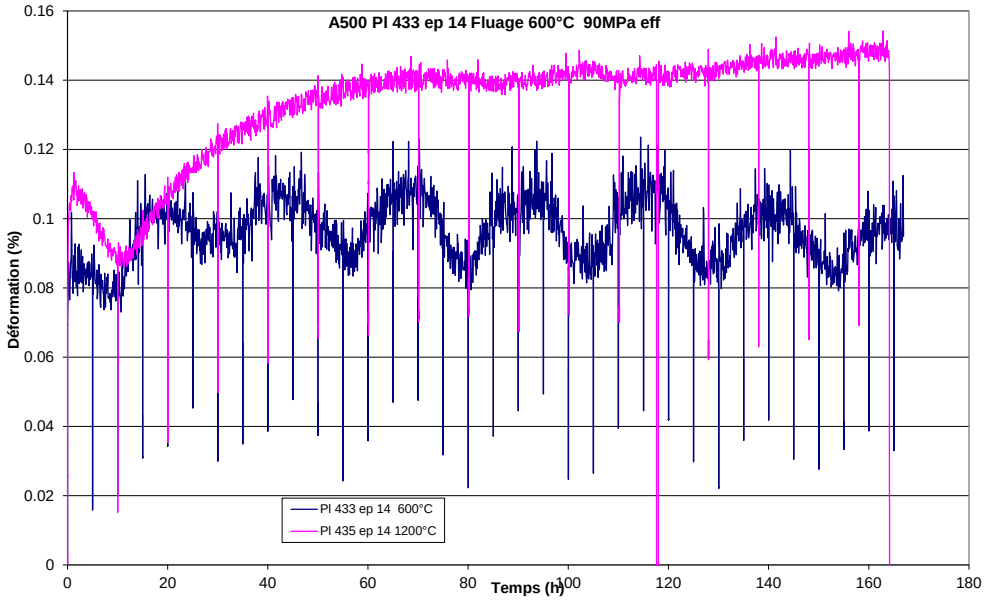

Figure 11. Strain Versus Time for A500 Loaded in Creep at 90 MPa (1200°C) and Fatigue at 90 MPa (600°C) for 160 Hours

3.4.5 Pre-conditioning: Creep

The parameters for pre-conditioning using creep loading were chosen considering the specific behavior of the A500 (i.e., no elastic domain) and the functioning of the self-sealing matrix. The parameters used for the creep conditioning were:

- Environment: Lab Air
- Stress Level: Efficient Stress of 90 MPa,
- Temperature: 1100°C,
- Duration: 30 hours.

The temperature of 1100°C was selected, as that is the maximum use temperature for A500 material as reported by SPS. A time of 30 hours was determined to be sufficient to thoroughly condition the material. Samples 28, 29 and 30 were pre-conditioned via creep at 1100ºC with an applied effective stress of 90 MPa for 30 hrs. All samples survived the creep exposure and the creep curves generated during this effort are shown in Figure 12. The samples show that no significant strain developed during the 30-hour test. All the samples exhibited very similar behavior, but one sample experienced a slight extensometer slip at about 5 hours into the test.

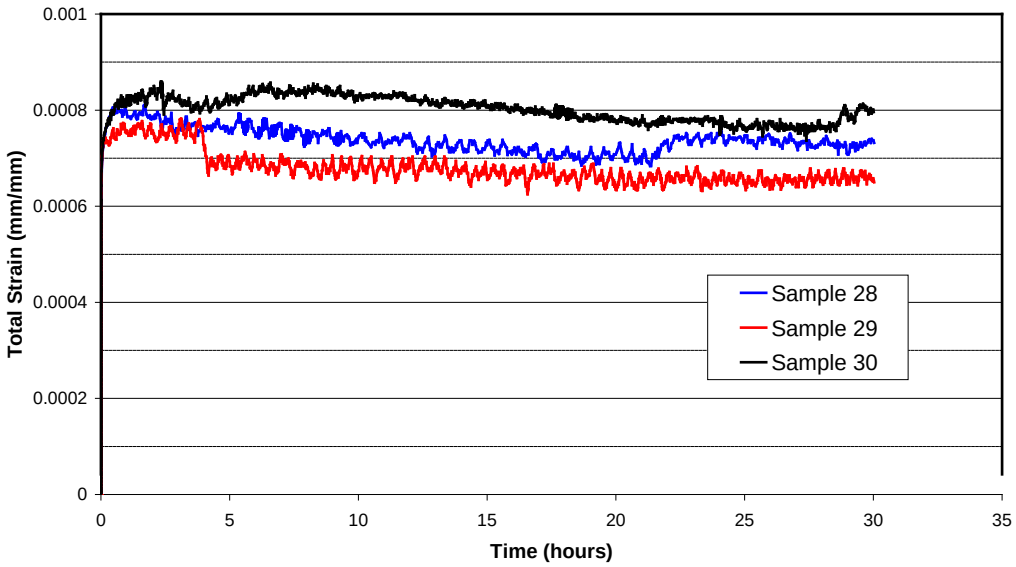

Figure 12. Strain Versus time Curve for Three Specimens Preconditioned via Creep

3.4.6 Pre-Conditioning – Fatigue.

The parameters for pre-conditioning by fatigue were chosen based on the material tensile properties. The plan was to load to approximately twice the proportional limit to saturate the number of matrix cracks. Past testing at SPS has shown that stiffness loss during fatigue loading occurs in the first few hundred cycles, so the test duration was limited to 1000 cycles. The parameters used were:

- Environment: Lab Air
- Stress Level: Efficient Stress of 150 MPa,
- Temperature: 23°C
- Duration: 1000 Cycles

Samples 31, 32 and 33 were fatigued at room temperature, at a maximum effective peak stress of 150 MPa for 1,000 cycles. All samples survived the fatigue tests. Efficient stress-strain curves for several of the fatigue cycles were captured during the tests and the results studied in order to determine the damage incurred. The peak strain for each loop is shown in Figure 13 which shows that all of the test specimens exhibited similar behavior. A plot showing efficient stress-versus-strain cycles for several different cycles for Sample 31 is given in Figure 14. There is a subtle shift in the loop location, indicating strain was accumulating in the sample. However, there is no clear way to visually note the presence of a slope shift that could indicate damage based on a modulus change. Curve fitting was done to a vast majority of the cycles and the damage parameter determined [based on $D = ((1-E_i)/E_o)$ where D is the damage parameter, E_i is the modulus per individual cycle, and E_o is the initial modulus] and is shown in Figure 15. The damage parameter appears to be leveling off starting at 800 cycles and suggests that the test specimens are saturated with micro-cracks.

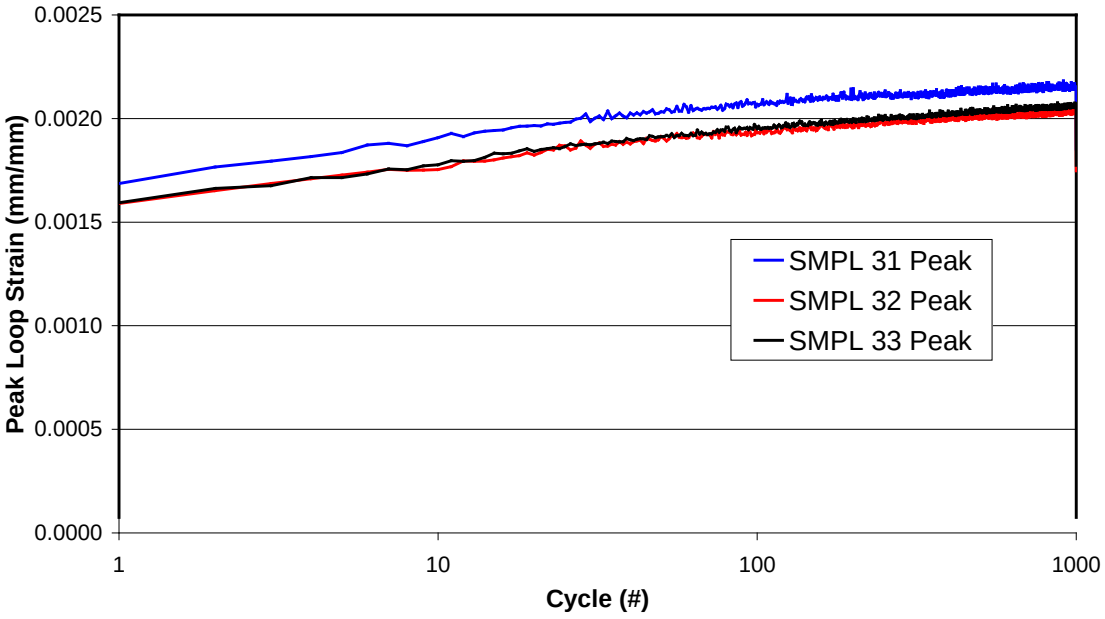

Figure 13. Peak Strain Versus Cycles for Three Specimens

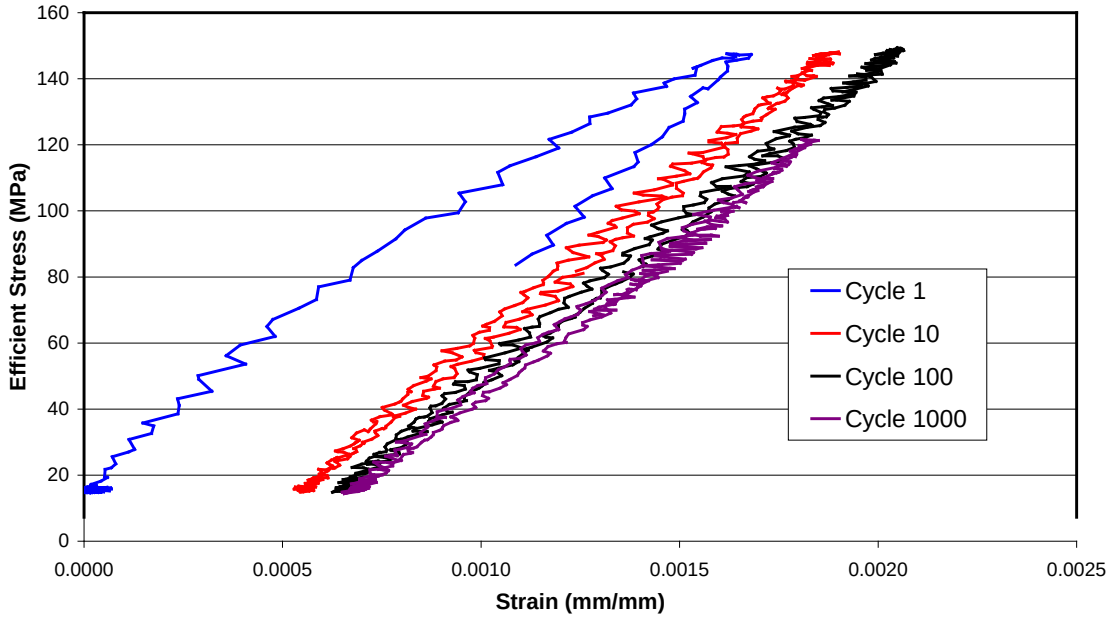

Figure 14. Cyclic Loop Data for Sample 31

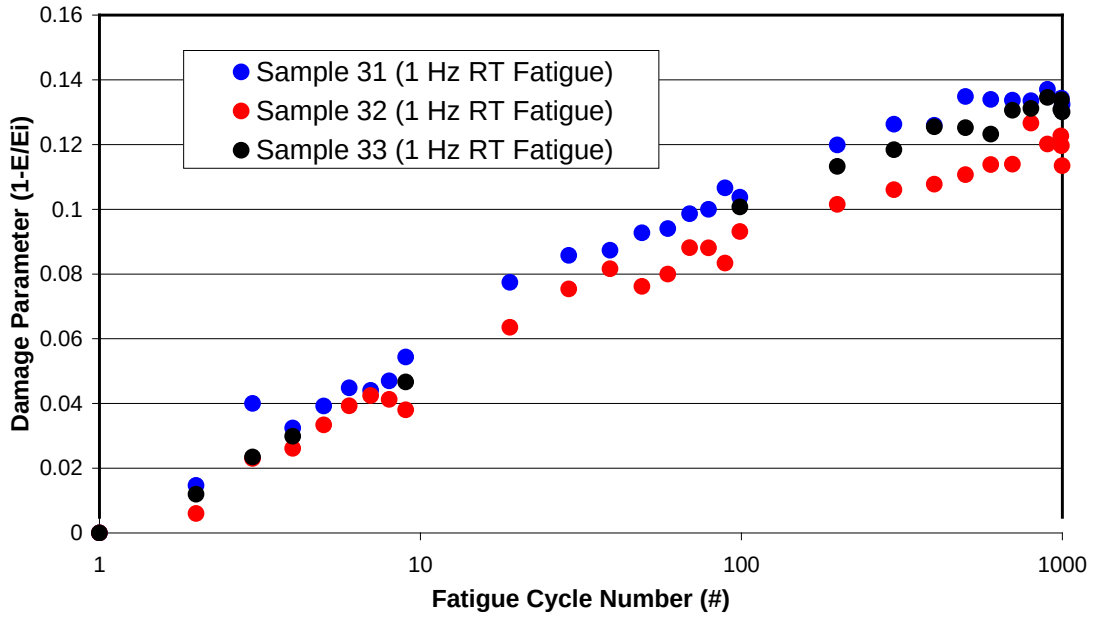

Figure 15. Damage Parameter Versus Cycle for Three Samples Subjected to 1 Hz Testing

3.4.7 Salt Fog Exposure.

The salt fog exposures were performed at NAVAIR following the procedures of ASTM B117. The designated specimens were exposed prior to the first burner rig cycle and then after every 12 major or 300 minor burner rig cycles. Section 3.5 discusses the burner rig cycles in more detail.

Each salt fog exposure was for a 24-hour duration. For the creep and fatigue pre-conditioned specimens, the salt fog exposure was applied after the pre-conditioning.

3.5 Burner Rig.

An atmospheric pressure Beacon burner rig system at NAVAIR was used to expose as-received, pre-conditioned, and salt fog-treated test specimens under conditions simulating the temperatures and temperature gradients of an afterburner during typical field usage [14,15]. Up to 12 test specimens were held circumferentially in a carousel and supported at their top and bottom. The carousel was positioned 8″(20 cm) from the flame and rotated at 100-200 rpm. The flame exited the combustor through a 2″-diameter circular nozzle and impinged upon the gage sections of the rotating 6″ coupons. The rig was calibrated by adjusting the primary to secondary air ratios to achieve a particular flame temperature for each set point, or maximum, temperatures in a given profile. The flame temperature was measured by a thermocouple. The volume of fuel was automatically controlled to attain the appropriate heating and/or cooling ramp rate. The test specimen temperature was monitored using a calibrated pyrometer and the temperature profile was recorded throughout the test. A photograph of the burner rig in operation is shown in Figure 16.

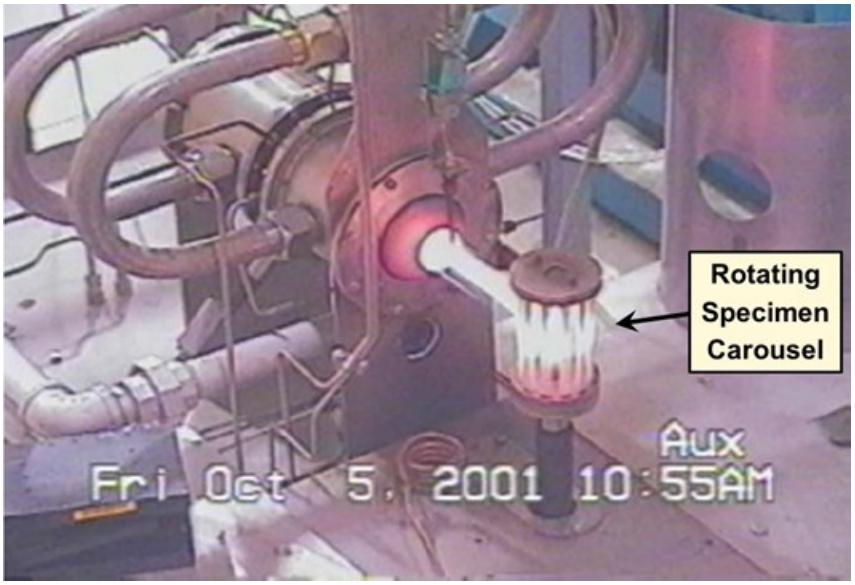

Figure 16. Optical Photograph of US Navy Burner Rig in Operation

Testing was performed using major cycles, each consisting of 25 minor cycles, which consisted of four temperature profiles, identified as C1-C4. As stated earlier, the temperature of the exhaust nozzle depends on how long the afterburner is operated. Therefore, the four temperatures selected covered the range of temperatures the seals might experience, with the maximum temperature limited to the reported use temperature for A500.

An example plot for a single cycle of each of the temperature profiles is shown in Figure 17 and shows both the time it took to reach each temperature and the time to cool to 1000°F. The maximum temperature and number of cycles that followed each temperature profile are given in

Table 4 and shown graphically in Figure 18. For each minor cycle, the carousel holding the specimens would rise up on an actuator and be impinged by the burner rig hot gas flow. Once the specimens reached the desired test temperature, the actuator was lowered and the carrousel moved out of the hot gas flow path. The specimens were allowed to cool to 1000°F before being inserted back into the hot gas flow. Each of the four temperatures took a different amount of time to reach the desired temperature, and the higher temperatures took longer to cool down to 1000°F. One sequence of the profiles (i.e., C1-C4), performed in order, made up one major cycle. In this study, the rig testing was interrupted following every 12 major, or 300 minor, increments for 24 hours of salt fog exposure or test specimen removal when applicable. The rig testing on this program consisted of up to 60 major cycles, which was the equivalent of 1500 minor cycles and approximately 57 hours of burner rig time.

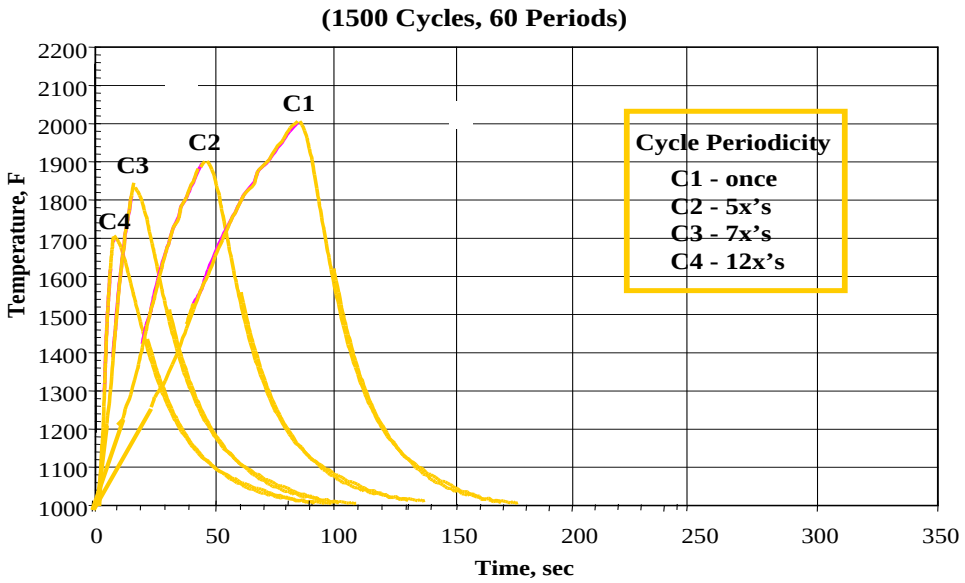

Figure 17. Example of the Burner Rig Temperature Profiles Used

Table 4. Major Burner Rig Cycle Description

Profile	Number of Cycles	Maximum Temperature (F)	Maximum Temperature (C)	Time (Minutes)
C1	1	2000	1093	4
C2	5	1900	1038	15
C3	7	1850	1010	14
C4	12	1700	927	24

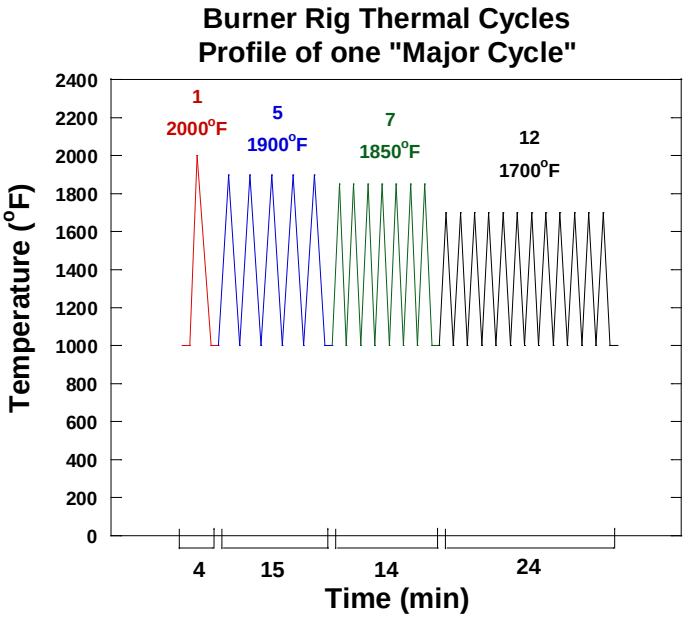

Figure 18. Schematic of Minor Thermal Cycles Making a Major Burner Rig Cycle

3.6 Test System SH#12.

The room temperature tensile testing following the burner rig testing was performed at multiple facilities. As previously stated, the tensile testing on as-manufactured material was performed by SPS (acceptance testing) and the USAF. After exposure, the specimens were subjected to room-temperature tensile testing using a loading rate of 0.0167 mm/s at multiple locations, including. These room temperature retained strength tension tests were performed by NAVAIR, Cincinnati Test Labs[1], and the USAF.

The tension tests performed by the USAF used a horizontal servo-hydraulic test system (SH#12). A photograph of the test system is shown in Figure 19. This test frame is uniquely orientated in the horizontal configuration and is equipped with custom-designed, water-cooled, friction-clamping grips; a MTS 609 alignment device; a 5.5-kip (25kN) MTS load cell; a MTS 458 analog Micro-Console signal controller; and University of Dayton Research Institute (UDRI)-developed MATE (material analysis and testing) test control and data acquisition software. This test frame was designed and built in the horizontal configuration specifically for characterization of the high-temperature mechanical properties of CMCs, which demonstrate less than 1% strain to failure.

Furnaces that operate in the vertical orientation experience “chimney” effects where the hot air rises and cooler air is drawn in from the bottom of the furnace. This causes the lower end of the gage section to always be cooler than the top end, making it difficult to generate a uniform temperature profile in this section of the test specimen. Multiple heating zones and strategic placement of insulation can mitigate only some of this effect. Furnaces operated with the specimen in the horizontal orientation produce a very symmetric and uniform temperature profile across the gage section of the test specimen. The horizontal configuration is also conducive to

[1] Cincinnati Test Lab, 1775 Carillon Boulevard, Cincinnati, Ohio 45240.

high-temperature strain measurement. The high-temperature extensometer mounting design requires substantially less spring force to keep the extensometer in contact with the test specimen, compared to when it is mounted in the vertical configuration.

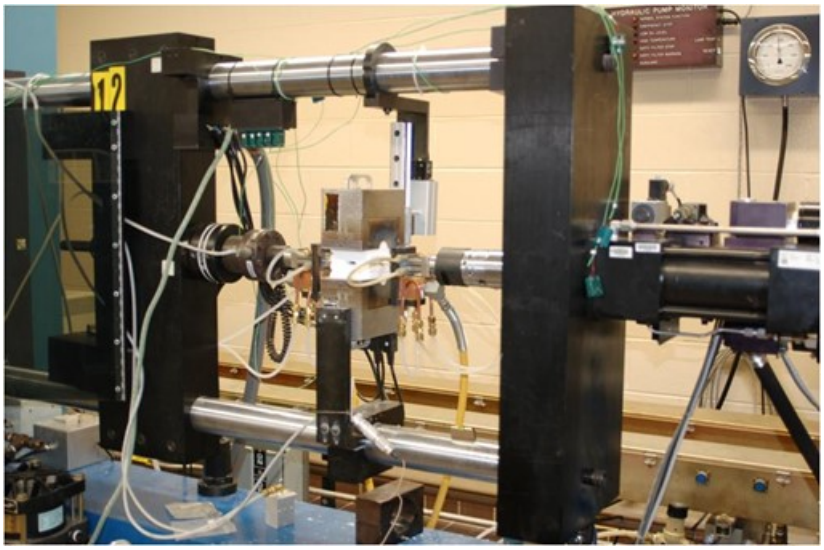

Figure 19. Photograph of the Horizontal Servo-Hydraulic Test System (SH#12) Used for Room- and Elevated-Temperature Testing

Other features to note on this test frame are the unique gripping system and the custom control and data-acquisition software. The grips were designed in-house to achieve a high degree of alignment while providing a fixed clamping condition at both ends of the specimen, ideal for strain-limited materials. These unique grips use a clamping action, driven by a pneumatic-to-hydraulic ram inside a yoke that goes around the grips, and applies the pressure normal to the grips. The grips require appropriately sized and prepared metal inserts to closely match the thickness of the test specimen, such that the grips flex less than a few thousandths of an inch. Once aligned, the system maintains alignment, and subsequent alignment checks are extremely repeatable. The inserts are either sandblasted or coated with a rough coating to maximize the coefficient of friction between the test specimen and the grip inserts. The grip bodies are cooled, while the metal inserts in contact with the specimen are not directly cooled. An MTS Model 609 device is used to align these grips by removing concentricity and angularity. Specialized test software allowed for real-time data acquisition and live display of multiple test parameters.

3.7 Verification of Alignment.

The grip/load train alignment was verified using a highly ground, hard steel, straight-sided specimen instrumented with eight strain gages, as shown in Figure 20. The goal for alignment was to be within ASTM specifications of less than 5% bending at 500 με displacement in all four specimen orientations. A plot of percent bending versus axial load is shown in Figure 21. Often, the percent bending at 500 με displacement was about only 2%.

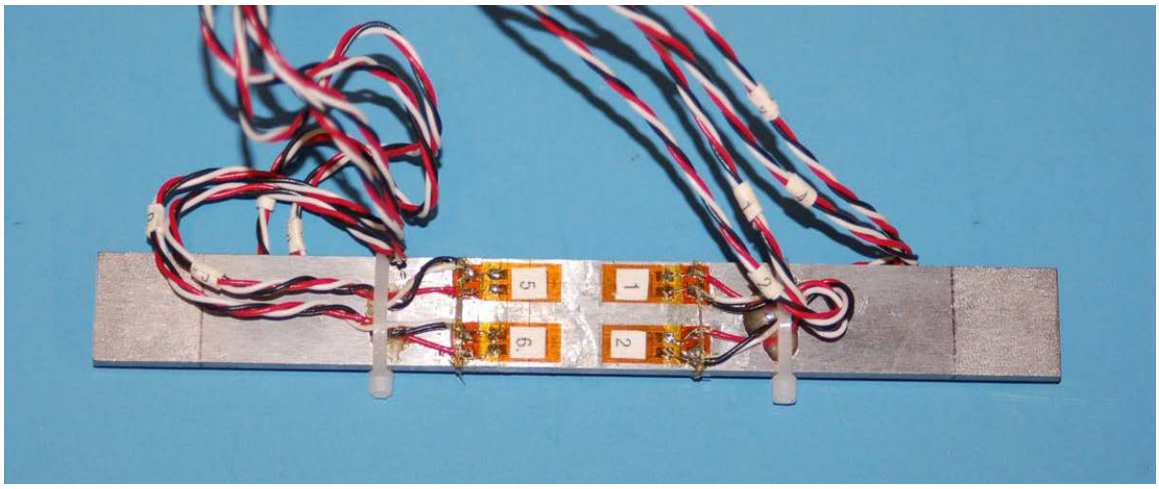

Figure 20. Strain-Gaged Steel Specimen Used to Verify Alignment of SH#12

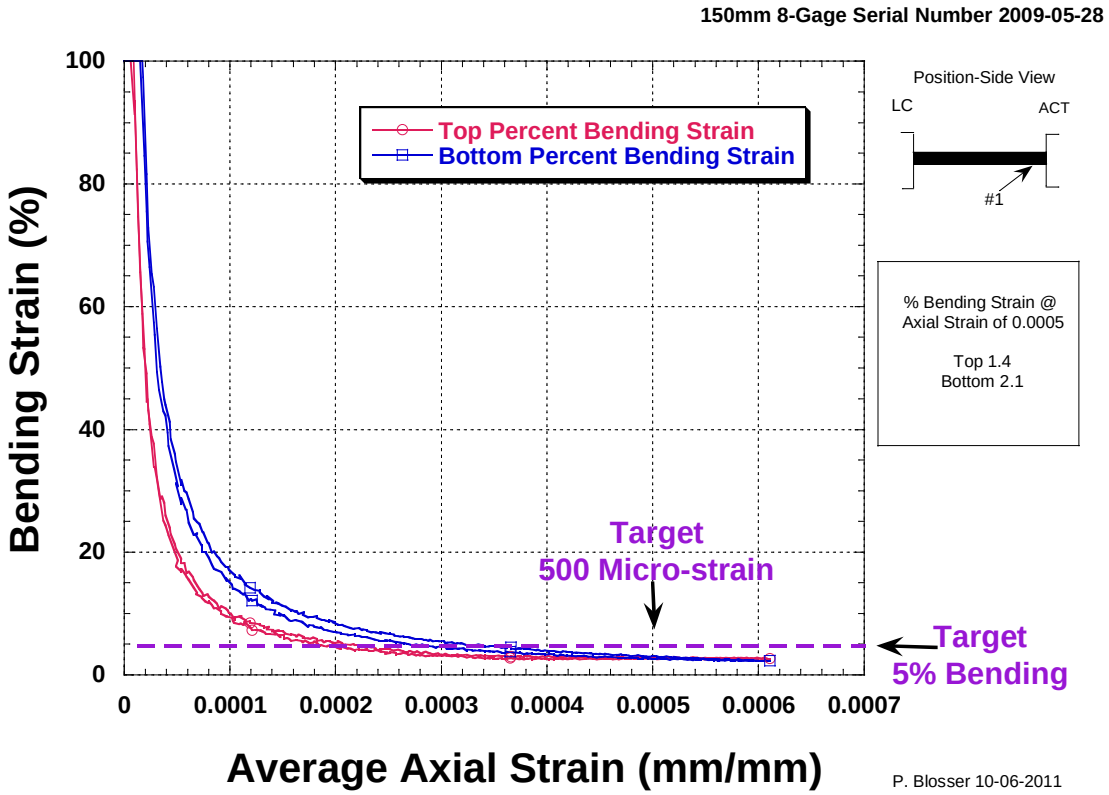

Figure 21. Bending Strain Versus Average Axial Strain for Alignment Check of SH#12

3.8 Reporting of Test Results.

Tensile properties are reported primarily as “efficient” properties, while in some cases “net” properties are also reported (as in the master Excel® spreadsheet attached to this report). The results of interest are the “efficient” properties, which are those calculated using only the hardening thickness of the material without including the external sequenced seal-coat layer. The hardening thickness of the materials used on this program was 2.6 mm. The “net” properties reported take into account the entire cross-section of the material, including the non-load-carrying thickness of the outer sequenced layer.

The efficient modulus reported is the slope of the efficient stress-versus-strain curve between zero load and an efficient stress of approximately 25 MPa. The proportional limit is the efficient stress level at which the linear regression, using the modulus as the slope, deviates from the efficient stress-versus-percent-strain curve by 10%. The percent strain at failure is also reported.

4.0 RESULTS

The results from the acceptance tension testing, burner rig plus salt fog, and pre-conditioning plus burner rig plus salt fog are discussed in the following sections. It is important to note that the USAF had an agreement with SPS that only microstructural studies could be performed – no elemental analysis was to be done on the specimens.

4.1 Acceptance Testing of As-Manufactured A500 C/SiC

SPS conducted acceptance tension testing to verify the quality of the A500 before sending test specimens out to be burner rig tested. The efficient tensile stress-versus-strain traces for the specimens oriented in the "1" direction are presented in Figure 22. Also shown on the plot is a representative "average" trace of the general stress-versus-strain behavior from the material database. The shapes of the curves are typical for the A500 material, in which there is no distinct transition from elastic to inelastic behavior. It is important to note that the results are shown in terms of the "efficient" properties. Figure 22 also shows that all of the tensile specimens exhibited superior tensile behavior to the average behavior for A500.

A summary of the average results is presented in Table 5 for the 0° or "1" direction coupons, the 90° or "2" direction, and for two of the larger test specimens. For comparison, Table 6 lists the statistical properties for A500 in the 0° ("1") direction and Table 7 lists the statistical properties in the 90° ("2") direction. From comparing the acceptance test data to the statistical database, it is clear that all of the panels easily exceeded the average properties.

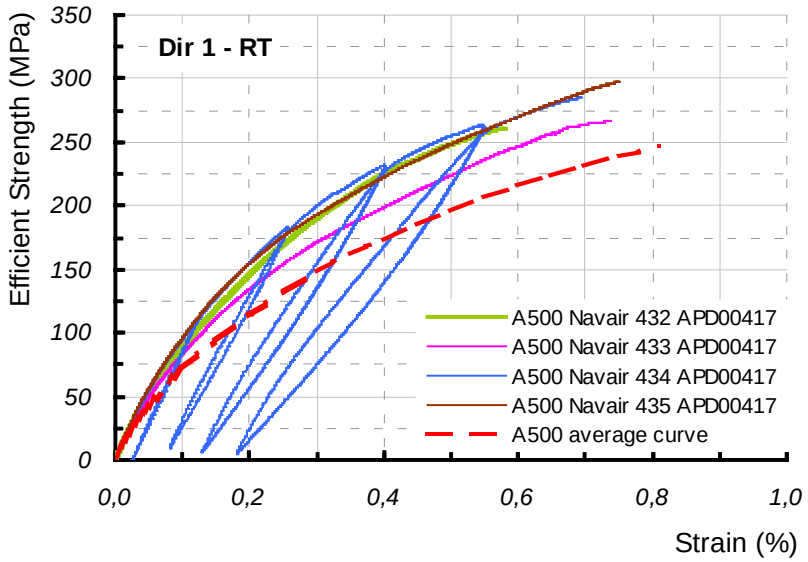

Figure 22. Efficient Stress Versus Strain for As-Manufactured A500 C/SiC Tested by SPS

Table 5. Average Tensile Properties for SPS A500 Acceptance Tests

Test Specimen Geometry	Specimen	Measured Thickness (mm)	Hardening Thickness (mm)	Modulus Efficient Stress (GPa)	Efficient Stress (MPa)	Strain to Failure (%)
dir. 1 - APD00417	432_10	3	2.6	127	265	0.58
	433_10	2.9	2.6	123	268	0.74
	434_10	3	2.6	127	285	0.69
	435_10	3.2	2.6	135	298	0.75
Average dir. 1 with APD00417				**128**	**279**	**0.69**
dir. 1 - APD11388	432_14	3	2.6	114	277	0.62
	434_14	3.05	2.6	129	282	0.69
Average dir. 1 with APD11388				**122**	**279**	**0.66**
dir. 2 - APD00417	432_15	3	2.6	115	298	0.8
	433_15	3	2.6	115	269	0.56
	434_15	3	2.6	110	0.8	0.8
	435_15	3.05	2.6	111	0.8	0.8
Average dir. 2 with APD00417				**113**	**142.03**	**0.74**

Extensometer: n°70816178, 25 mm gage length on Instron 1185 H4224
For failure location, the gage section stretched from x mm to x mm along length)
Test Temperature: Room Temperature
Specimen: c.f. APD00417 and APD11388 plan
Efficient strength calculated using a hardening thickness of 2.6mm
Loading rate: 0.0167 mm/second, which is 1 mm/minute

Table 6. Average Tensile Properties for A500 Oriented in "1" Direction

$-\sigma r1_{[eff]\ av.} = 252$ MPa ($\sigma = 27$ MPa)	$-\varepsilon r1_{av.} = 0.82$ % ($\varepsilon = 0.09$ %)
$-[\sigma r1_{[eff]\ av.} - 3\sigma] = 170$ MPa	$-[\varepsilon r1_{av.} - 3\varepsilon] = 0.55$ %

Table 7. Average Tensile Properties for A500 Oriented in "2" Direction

$-\sigma r2_{[eff]\ av.} = 264$ MPa ($\sigma = 17$ MPa)	$-\varepsilon r2_{av.} = 0.83$ % ($\varepsilon = 0.11$ %)
$-[\sigma r2_{[eff]\ av.} - 3\sigma] = 213$ MPa	$-[\varepsilon r2_{av.} - 3\varepsilon] = 0.50$ %

The USAF also conducted acceptance tension testing on three as-manufactured test specimens prior to any exposure and a plot of efficient stress versus strain is shown in Figure 23. The curves are typical of the A500 material and exhibit no distinct initial elastic region, making calculation of a modulus value difficult.

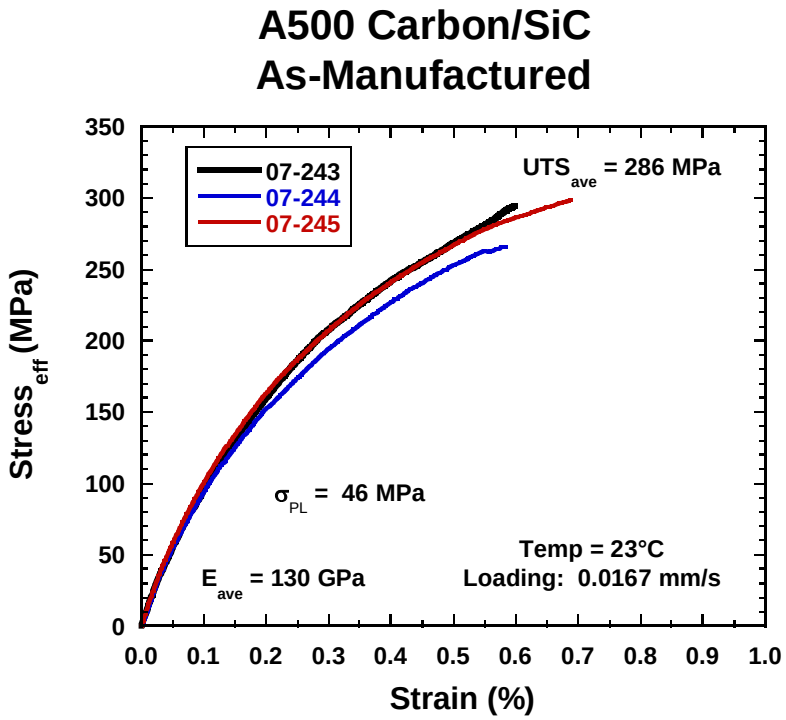

Figure 23. Efficient Stress Versus Strain for As-Manufactured A500 C/SiC Tested by USAF

All seven of the tensile test results on the as-manufactured material are listed in Table 8 and include both the acceptance test data for each plate measured by SPS and the tensile data measured by the USAF. The USAF took the raw tensile stress-versus-strain data supplied by SPS and analyzed it using the same procedure as their test results. Averages for the efficient tensile strength, efficient proportional limit, efficient modulus, and strain at failure, as measured by the two facilities, are nearly identical and consistent with the database for the A500 C/SiC CMC material. This was good to document and gave the green light to proceed with the burner rig experiments.

Table 8. As-Manufactured Tensile Properties for A500 C/SiC Tested by SPS and USAF

Specimen Identification SNECMA	Specimen Identification NAVAIR	Specimen Identification AIR FORCE	Pre-conditioning	Salt Exposure (Yes/No)	Salt Exposure (# / Hrs)	Burner Rig Cycles (#)	Hardening Thickness (mm)	UTS Efficient (MPa)	PL Efficient (MPa)	Modulus Efficient (GPa)	Strain to Failure (%)
432-10	---	---	As-Processed	No	0 / 0	0	2.6	260.5	39.5	120.2	0.58
433-10	---	---	As-Processed	No	0 / 0	0	2.6	266.9	35.0	117.2	0.74
434-10	---	---	As-Processed	No	0 / 0	0	2.6	285.3	48.9	124.1	0.69
435-10	---	---	As-Processed	No	0 / 0	0	2.6	298.2	46.7	130.8	0.75
Average								**277.7**	**42.5**	**123.1**	**0.73**
Stdev								17.23	6.43	5.87	0.032
432-5	25	07-243*	As-Processed	No	0 / 0	0	2.6	294.0	43.0	126.0	0.60
433-5	26	07-244*	As-Processed	No	0 / 0	0	2.6	266.0	46.2	130.9	0.58
434-5	27	07-245*	As-Processed	No	0 / 0	0	2.6	298.9	49.1	132.8	0.69
Average								**286.3**	**46.1**	**129.9**	**0.62**
Stdev								17.75	3.05	3.51	0.059

* = the following test parameters
Extensometer: Quartz Rod, 15 mm gage length
For failure location, the gage section stretched from x mm to x mm along length)
Test Temperature: Room Temperature
Specimen: Length = 175 mm, Width 12 mm, Gage Length = 28 mm, Gage Width = 8 mm, Radius = 368 mm
Efficient strength calculated using a hardening thickness of 2.6 mm
Modulus determined using a stress window of approximately 0 - 25 MPa
Proportional Limit = stress at 10% deviation between the effcient stress and the predicted stress
Loading rate: 0.0167 mm/second, which is 1 mm/minute

4.2 Burner Rig Plus Salt Fog Exposure

The samples tested under this portion of the test matrix saw salt fog exposure in conjunction with increasing numbers of burner rig cycles in order to identify the level that produces a measurable degradation in properties. A total of five increments of burner rig cycles were evaluated (300, 600, 900, 1200, and 1500 cycles) with corresponding amounts of salt fog exposures (24, 48, 72, 96, and 120 hours), respectively.

The retained tensile properties from the burner rig- and salt fog-exposed specimens are compared against the results of the seven tension tests conducted on as-manufactured material in Table 9, as well as presented in several plots. Figure 24 is plot of efficient UTS versus cycles. Tensile strength remains unaffected and constant up to 600 cycles, but at 900 cycles, there is a slight (5%) decrease in strength, with strength decreasing 11% at 1200 cycles. and 29% at 1500 cycles. A plot of efficient modulus-versus-burner rig cycles is shown in Figure 25. Stiffness remained constant up to 1200 cycles, but decreased significantly at 1500 cycles, indicating damage to the carbon fibers. Strain to failure is shown in Figure 26 and remained constant up to 900 cycles, but decreased at 1200 cycles, and continued to decrease at 1500 cycles. Thus, by 1200 cycles, there was some localized damage occurring to the carbon fibers. However, overall, there was good strain to failure and no sign of embrittlement. These results suggest that the A500 C/SiC CMC performed extremely well up to 900 burner rig plus salt fog cycles, after which, there was a progressive decrease in tensile properties with further cycles.

Table 9. Retained Tensile Properties Following Burner Rig Plus Salt Fog Exposure

Specimen Identification SNECMA	Specimen Identification NAVAIR	Specimen Identification AIR FORCE	Pre-conditioning	Salt Exposure (# / Hrs)	Burner Rig Cycles (#)	Hardening Thickness (mm)	UTS Efficient (MPa)	PL Efficient (MPa)	Modulus Efficient (GPa)	Strain to Failure (%)
432-10	---	---	As-Processed	0 / 0	0	2.6	260.5	39.5	120.2	0.58
433-10	---	---	As-Processed	0 / 0	0	2.6	266.9	35.0	117.2	0.74
434-10	---	---	As-Processed	0 / 0	0	2.6	285.3	48.9	124.1	0.69
435-10	---	---	As-Processed	0 / 0	0	2.6	298.2	46.7	130.8	0.75
Average							**277.7**	**42.5**	**123.1**	**0.73**
Stdev							17.23	6.43	5.87	0.032
432-5	25	07-243*	As-Processed	0 / 0	0	2.6	294.0	43.0	126.0	0.60
433-5	26	07-244*	As-Processed	0 / 0	0	2.6	266.0	46.2	130.9	0.58
434-5	27	07-245*	As-Processed	0 / 0	0	2.6	298.9	49.1	132.8	0.69
Average							**286.3**	**46.1**	**129.9**	**0.62**
Stdev							17.75	3.05	3.51	0.059
432-4	1	07-196*	As-Processed	1 / 24	300	2.6	278.7	43.4	131.3	0.67
434-8	2	07-197*	As-Processed	1 / 24	300	2.6	292.9	38.9	129.7	0.82
435-7	3	07-198*	As-Processed	1 / 24	300	2.6	283.3	45.7	143.8	0.66
Average	**Average**	**Average**					**285.0**	**42.7**	**134.9**	**0.72**
Stdev	Stdev	Stdev					7.27	3.46	7.72	0.090
432-7	13	07-199*	As-Processed	2 / 48	600	2.6	275.7	45.9	131.9	0.74
433-8	14	07-200*	As-Processed	2 / 48	600	2.6	292.8	39.1	143.3	0.63
435-2	15	07-201*	As-Processed	2 / 48	600	2.6	307.2	45.1	137.2	0.76
Average	**Average**	**Average**					**291.9**	**43.4**	**137.5**	**0.71**
Stdev	Stdev	Stdev					15.80	3.73	5.70	0.070
432-6	4	07-202*	As-Processed	3 / 72	900	2.6	281.3	37.8	129.6	0.80
434-7	5	07-203*	As-Processed	3 / 72	900	2.6	248.4	37.0	134.2	0.64
435-5	6	07-204*	As-Processed	3 / 72	900	2.6	285.7	42.6	136.2	0.64
Average	**Average**	**Average**					**271.8**	**39.1**	**133.3**	**0.69**
Stdev	Stdev	Stdev					20.34	3.03	3.38	0.092
432-3	16	07-205*	As-Processed	4 / 96	1200	2.6	259.4	39.4	126.4	0.51
433-7	17	07-206*	As-Processed	4 / 96	1200	2.6	229.9	41.5	127.3	0.50
435-8	18	07-207*	As-Processed	4 / 96	1200	2.6	270.0	38.5	149.3	0.68
Average	**Average**	**Average**					**253.1**	**39.8**	**134.3**	**0.60**
Stdev	Stdev	Stdev					20.76	1.54	12.97	0.120
432-1	7	---	As-Processed	5 / 120	1500	2.6	213.4	78.3	124.2	0.29
433-2	8	---	As-Processed	5 / 120	1500	2.6	209.5	40.3	110.7	0.58
433-1	9	---	As-Processed	5 / 120	1500	2.6	186.1	42.4	99.4	0.41
Average	**Average**	**Average**					**203.0**	**53.7**	**111.4**	**0.43**
Stdev	Stdev	Stdev					14.76	21.36	12.42	0.146

* = the following test parameters
Extensometer: Quartz Rod, 15 mm gage length
For failure location, the gage section stretched from x mm to x mm along length)
Test Temperature: Room Temperature
Specimen: Length = 175 mm, Width 12 mm, Gage Length = 28 mm, Gage Width = 8 mm, Radius = 368 mm
Efficient strength calculated using a hardening thickness of 2.6 mm
Modulus determined using a stress window of approximately 0 - 25 MPa
Proportional Limit = stress at 10% deviation between the effcient stress and the predicted stress
Loading rate: 0.0167 mm/second, which is 1 mm/minute

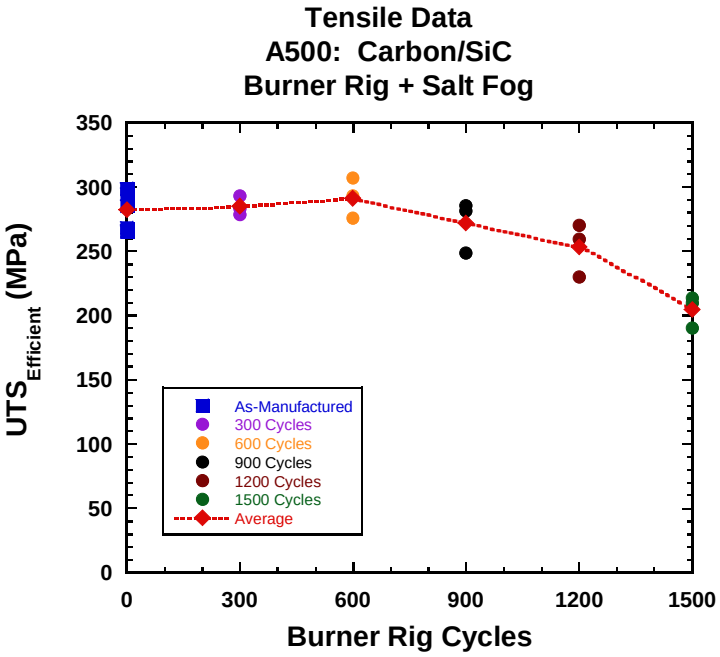

Figure 24. Efficient Stress Versus Burner Rig Cycles for A500 C/SiC Following Various Burner Rig and Salt Fog Exposure Durations

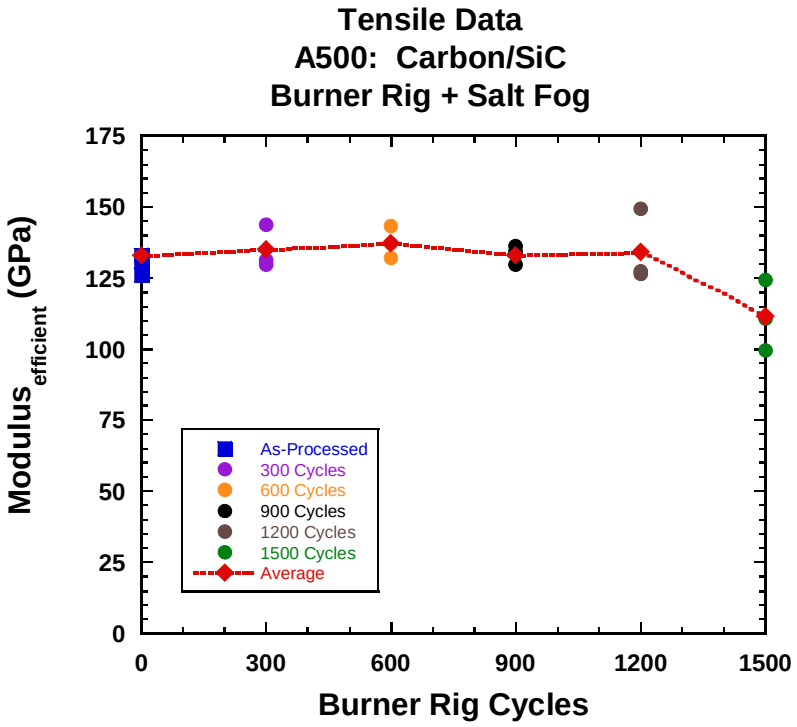

Figure 25. Modulus Versus Burner Rig Cycles for A500 C/SiC Following Various Burner Rig and Salt Fog Exposure Durations

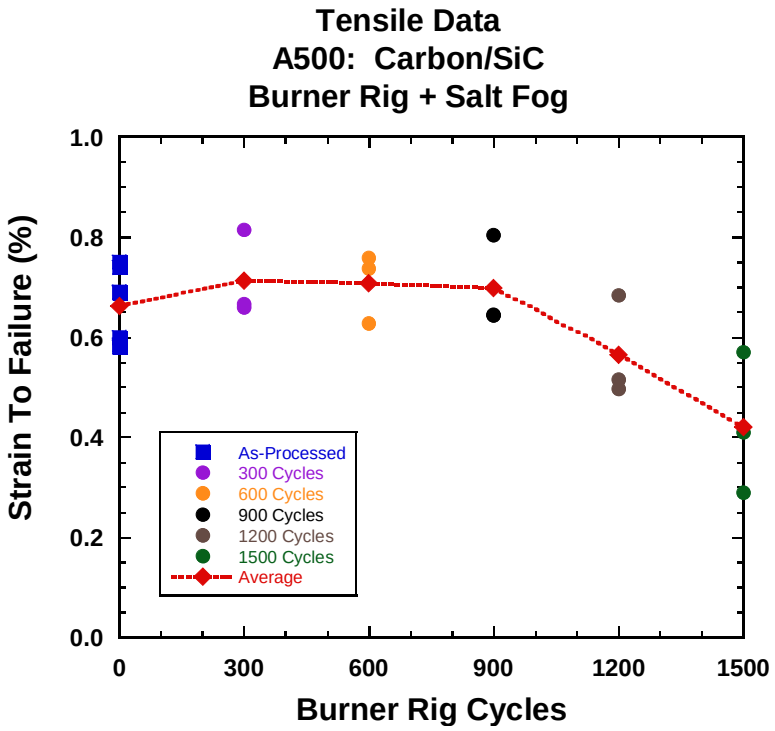

Figure 26. Strain to Failure Versus Burner Rig Cycles for A500 C/SiC Following Various Burner Rig and Salt Fog Exposure Durations

A representative efficient stress-strain curve for each of the different exposure durations tested is shown in Figure 27. The plot shows that, at 1200 burner rig cycles plus salt fog exposure, there is a measureable drop in strength; however, at 1500 cycles, there is both a drop in strength and a very pronounced decrease in stiffness, as well as a slight decrease in strain to failure. Thus, it appears that the sealing phases incorporated into the A500 CMC perform well up to 900 to 1200 burner rig plus salt fog cycles, but by 1500 cycles, they have been exhausted and the degradation has started to accelerate with continued cycling.

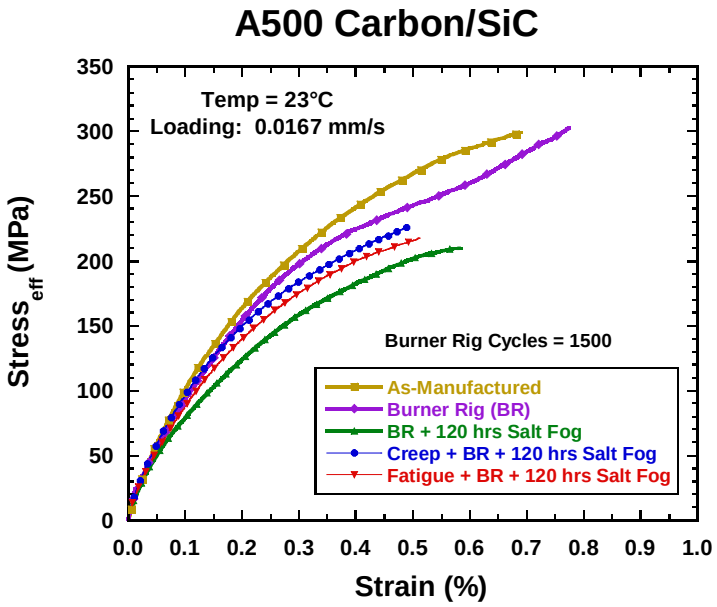

Figure 27. Tensile Stress-Versus-Strain Behavior for A500 Following Various Burner Rig and Salt Fog Exposure Durations

The samples tested under burner rig plus salt fog were documented using optical photography following exposure and tension testing. The aim was to document the surfaces of the test specimens with respect to the formation of any reactive phases or degradation.

Figure 28 shows a failed as-manufactured tensile specimen and Figure 29 shows a higher magnification optical photograph of the surface of the gage section of the tensile specimen. There was nothing noteworthy to report about the surface of the test specimen, other than a few stray fibers coated with a thick layer of matrix.

Figure 30 shows a failed tensile specimen that saw 300 burner rig cycles plus 24 hours of salt fog exposure, and Figure 31 shows a higher magnification of the gage section of the tensile specimen. The only difference between this specimen and the as-manufactured specimen is that it appears to be a bit darker. Other than that no other differences could be observed.

Figure 32 shows a failed tensile specimen that saw 600 burner rig cycles plus a total of 48 hours of salt fog exposure, and Figure 33 shows a higher magnification of the gage section of the tensile specimen. Here, at 600 cycles one can observe a distinct cracking pattern in the higher magnification image and that the cracks appear to be filled in with a thin layer of white material. We know from SEM work that this white material is actually a foamy glass that is a by-product of the sealing phases in the matrix reacting with the moisture and salt during the burner rig exposures.

Figure 34 shows a failed tensile specimen that saw 900 burner rig cycles plus a total of 72 hours of salt fog exposure, and Figure 35 shows a higher magnification of the gage section of the tensile specimen. Here, at 900 cycles, there is more of the glassy phase filling in the cracks, and appears to now be flowing and spreading onto the surface of the test specimen.

Figure 36 shows a failed tensile specimen that saw 1200 burner rig cycles plus a total of 96 hours of salt fog exposure, and Figure 37 shows a higher magnification of the gage section of the tensile specimen. Here, at 1200 cycles, there is a significantly more of the glassy phase filling in the cracks and on the surface, to the point where it can even be seen in the low-magnification image of the failed tensile specimen. In addition, it is suggested that the number of the matrix cracks appears to have increased slightly.

Figure 38 shows a failed tensile specimen that saw 1500 burner rig cycles plus a total of 120 hours of salt fog exposure, and Figure 39 shows a higher magnification of the gage section of the tensile specimen. Here, at 1500 cycles, there is a very large amount of the glassy phase, not only filling in the cracks, but now the cracks appear to have widened significantly. In addition, the density of the matrix cracks appears to have increased. In the low-magnification image of the failed specimen, the amount of glassy phase has significantly increased and the strips of glassy phase have clearly widened.

The condition of the surfaces of the tested specimens clearly matches up with the tensile test results. Up to about 900 cycles, there is little sign of degradation occurring on the surfaces of the test specimens. However, at 1200 and 1500 cycles, there is significant glass formation that continues to grow and widen in the cracks, indicating continued degradation is occurring as burner rig cycles increase past 900 cycles.

Figure 28. Optical Photograph of Tension-Tested As-Manufactured A500 C/SiC Sample (#07-245)

Figure 29. Optical Photograph Surface of Gage Section of As-Manufactured A500 C/SiC Sample – (#07-245)

Figure 30. Optical Photograph Of A Tension-Tested A500 C/SiC Sample (#3) After 300 Burner Rig Cycles and 24 Hours Salt Fog Exposure

Figure 31. Optical Photograph Of A Tension-Tested A500 C/SiC Sample (#3) After 300 Burner Rig Cycles and 24 Hours Salt Fog Exposure

Figure 32. Optical Photograph of a Tension-Tested A500 C/SiC Sample (#13) After 600 Burner Rig Cycles and 48 Hours Salt Fog Exposure

Figure 33. Optical Photograph of a Tension-Tested A500 C/SiC Sample (#13) After 600 Burner Rig Cycles and 48 Hours Salt Fog Exposure

Figure 34. Optical Photograph of a Tension-Tested A500 C/SiC Sample (#4) After 900 Burner Rig Cycles and 72 Hours Salt Fog Exposure

Figure 35. Optical Photograph of a Tension-Tested A500 C/SiC Sample (#4) After 900 Burner Rig Cycles and 72 Hours Salt Fog Exposure

Figure 36. Optical Photograph of a Tension-Tested A500 C/SiC Sample (#16) After 1200 Burner Rig Cycles and 96 Hours Salt Fog Exposure

Figure 37. Optical Photograph of a Tension-Tested A500 C/SiC Sample (#16) After 1200 Burner Rig Cycles and 96 Hours Salt Fog Exposure

Figure 38. Optical Photograph of a Tension-Tested A500 C/SiC Sample (#8) After 1500 Burner Rig Cycles and 120 Hours Salt Fog Exposure

Figure 39. Optical Photograph of a Tension-Tested A500 C/SiC Sample (#8) After 1500 Burner Rig Cycles and 120 Hours Salt Fog Exposure

4.3 Pre-conditioning Plus Buner Rig Plus Salt Fog Exposure

This portion of the test matrix evaluated the effect of pre-conditioning the test samples before running the burner rig plus salt fog exposures. As stated earlier, pre-conditioning, either by creep or fatigue, was performed prior to the first salt fog exposure. The salt fog exposure was performed prior to burner rig testing and then after every 300 minor burner rig cycles. Test specimens were subjected to 1500 burner rig cycles and a total of 120 hours salt fog exposure.

The retained tensile properties from all of the conditioned burner rig-tested specimens are listed in Table 10. Included in the table are results from as-manufactured material, the test specimens that saw only 1500 burner rig cycles, and the pre-conditioned specimens that were exposed to the 1500 burner rig cycles and the 120 hours of salt fog exposure. A quick study of the tensile data reveals that the tensile strength values for the burner rig only tests are nearly identical to those of the as-manufactured specimens. However, the burner rig plus salt fog exposure significantly reduced tensile strength and was true for both un-conditioned plus salt fog and pre-conditioned plus salt fog.

The tensile data from the table can also be presented in the form of bar charts. Figure 40 presents efficient strength versus test condition. The data to the left of the dashed line on each of the following bar charts are from the as-manufactured material and the specimens that saw 1500 burner rig cycles with no salt fog exposure. To the right of the dashed line are the specimens that saw 1500 burner rig cycles and 120 hours of salt fog exposure, with and without pre-

conditioning. As stated above, the 1500 burner rig cycles had no effect on retained tensile strength, which is an excellent result for the A500 CMC. This documents that thermal cycling, even in the presence of a hot gas flow path that contains significant moisture, does not result in any loss in strength; thus, making the A500 CMC a prime candidate for aerospace turbine engine exhaust nozzle applications. However, the introduction of salt fog does result in degradation, which produces a ~25%-30% decrease in retained tensile strength. The percentage loss in strength was essentially the same for all three salt fog conditions. The samples that saw burner rig plus salt fog lost the same amount of strength as the samples that were preconditioned with either fatigue loading or creep loading, demonstrating that pre-conditioning has no effect. It is the 120 hours of salt fog exposure combined with the burner rig that resulted in the strength loss. The introduction of salt fog exposure produces reactions that are aggressive enough to overcome the material's protection mechanisms after 1500 burner rig cycles and 120 hours of salt fog exposure.

Table 10. Retained Tensile Properties for Pre-conditioned Test Specimens Exposed to 1500 Burner Rig Cycles and 120 Hours Salt Fog Exposure

Specimen Identification SNECMA	Specimen Identification NAVAIR	Specimen Identification AIR FORCE	Pre-conditioning	Salt Exposure (# / Hrs)	Burner Rig Cycles (#)	Hardening Thickness (mm)	UTS Efficient (MPa)	PL Efficient (MPa)	Modulus Efficient (GPa)	Strain to Failure (%)
432-10	---	---	As-Processed	0 / 0	0	2.6	260.5	39.5	120.2	0.58
433-10	---	---	As-Processed	0 / 0	0	2.6	266.9	35.0	117.2	0.74
434-10	---	---	As-Processed	0 / 0	0	2.6	285.3	48.9	124.1	0.69
435-10	---	---	As-Processed	0 / 0	0	2.6	298.2	46.7	130.8	0.75
Average							**277.7**	**42.5**	**123.1**	**0.73**
Stdev							17.23	6.43	5.87	0.032
432-5	25	07-243*	As-Processed	0 / 0	0	2.6	294.0	43.0	126.0	0.60
433-5	26	07-244*	As-Processed	0 / 0	0	2.6	266.0	46.2	130.9	0.58
434-5	27	07-245*	As-Processed	0 / 0	0	2.6	298.9	49.1	132.8	0.69
Average							**286.3**	**46.1**	**129.9**	**0.62**
Stdev							17.75	3.05	3.51	0.059
432-2	10	---	As-Processed	0 / 0	1500	2.6	302.7	35.0	153.0	0.61
434-1	11	---	As-Processed	0 / 0	1500	2.6	302.6	28.0	161.0	0.78
433-9	12	---	As-Processed	0 / 0	1500	2.6	279.0	117.7	92.8	0.78
Average	**Average**	**Average**					**294.7**	**60.2**	**135.6**	**0.72**
Stdev	Stdev	Stdev					13.65	49.89	37.28	0.098
432-1	7	---	As-Processed	5 / 120	1500	2.6	213.4	78.3	124.2	0.29
433-2	8	---	As-Processed	5 / 120	1500	2.6	209.5	40.3	110.7	0.58
433-1	9	---	As-Processed	5 / 120	1500	2.6	186.1	42.4	99.4	0.41
Average	**Average**	**Average**					**203.0**	**53.7**	**111.4**	**0.43**
Stdev	Stdev	Stdev					14.76	21.36	12.42	0.146
433-3	28	---	Creep**	5 / 120	1500	2.6	185.5	41.2	92.4	0.79
434-3	29	---	Creep**	5 / 120	1500	2.6	225.6	44.9	127.0	0.49
435-3	30	---	Creep**	5 / 120	1500	2.6	244.6	47.5	123.0	0.83
Average	**Average**	**Average**					**218.6**	**44.5**	**114.1**	**0.70**
Stdev	Stdev	Stdev					30.20	3.17	18.93	0.186
433-6	31	---	Fatigue***	5 / 120	1500	2.6	191.6	41.4	92.2	0.56
434-6	32	---	Fatigue***	5 / 120	1500	2.6	217.2	35.0	123.1	0.51
435-6	33	---	Fatigue***	5 / 120	1500	2.6	229.7	35.4	119.0	0.73
Average	**Average**	**Average**					**212.8**	**37.3**	**111.4**	**0.60**
Stdev	Stdev	Stdev					19.42	3.59	16.78	0.115

* = the following test parameters
Extensometer: Quartz Rod, 15 mm gage length
For failure location, the gage section stretched from x mm to x mm along length)
Test Temperature: Room Temperature
Specimen: Length = 175 mm, Width 12 mm, Gage Length = 28 mm, Gage Width = 8 mm, Radius = 368 mm
Efficient strength calculated using a hardening thickness of 2.6 mm
Modulus determined using a stress window of approximately 0 - 25 MPa
Proportional Limit = stress at 10% deviation between the effcient stress and the predicted stress
Loading rate: 0.0167 mm/second, which is 1 mm/minute
** = creep tests at 1100ºC and 90 MPa for 30 hrs
*** = RT 1 Hz Fatigue Test at 150 MPa for 1000 cycles

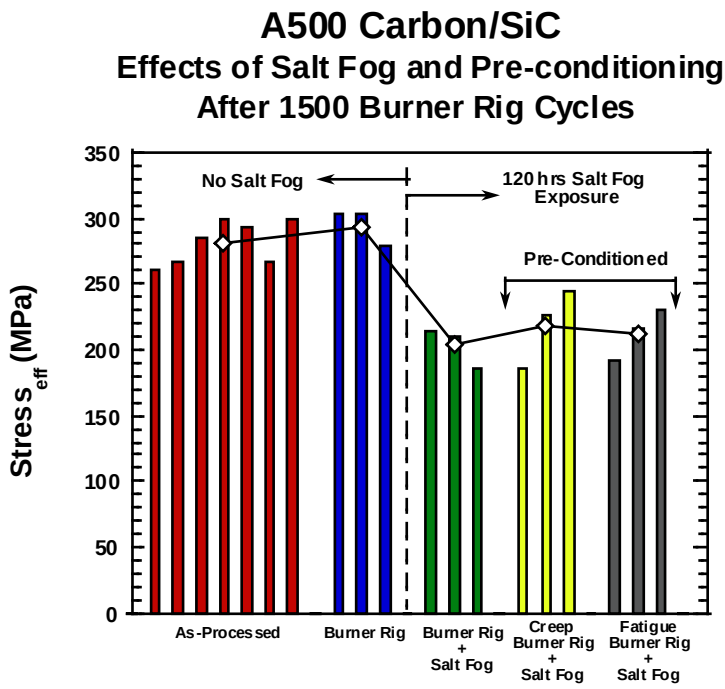

Figure 40. Efficient Stress Versus Test Condition for A500 C/SiC

The A500 CMC stress-versus-strain data typically exhibits a very small initial linear region, making it difficult to calculate a modulus value. All modulus value calculations used the same stress range of 5 MPa to 25 MPa. Retained stiffness is useful in determining how much degradation has occurred to the carbon fibers. A bar chart of modulus versus test conditions is shown in Figure 41, which shows that the modulus values follow a similar trend to the ultimate tensile strength. The burner rig testing alone did not result in any decrease in stiffness; if anything, stiffness actually increased significantly for two specimens that only saw1500 burner rig cycles. The third specimen exhibited a very low modulus value that is way out of line with all of the others; presumably a result of an issue with the tension test equipment, but the authors have no direct evidence for censoring the data. However, the three burner rig conditions that incorporated salt fog all experienced an approximately 14% decrease in measured modulus. There was no difference between pre-conditioned specimens and those that only saw the burner rig plus salt fog exposures. This result is a bit surprising, since the fatigue pre-conditioned specimens were fatigued at 150 MPa for 1000 cycles which, in other CMCs, fatigue loading would result in a low modulus value. It is suggested that the loss in stiffness for the three test conditions that involved salt fog can be attributed to damage to the carbon fibers by the salt reacting during the burn rig exposure. This observation is supported by the fact that the burner rig specimens without salt fog exposure experienced no loss in stiffness.

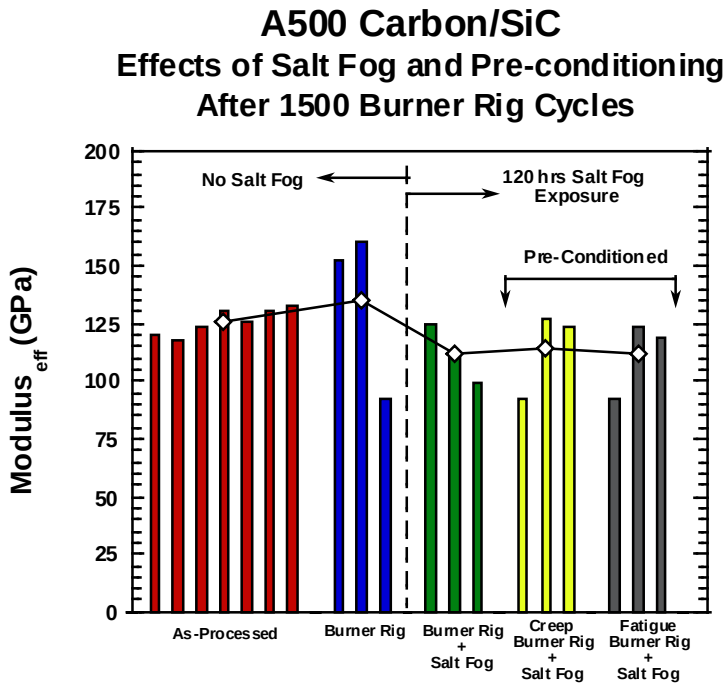

Figure 41. Modulus Versus Test Condition for A500 C/SiC

As stated earlier, the tensile stress-versus-strain behavior of A500 does not exhibit a well-defined initial linear region and the transition from linear to non-linear stress-versus-strain behavior is very subtle, making it sometimes difficult to calculate a proportional limit. Figure 42shows that the proportional limit values are all very similar and independent of test type. One of the specimens tested for 1500 burner rig cycles exhibited a very high proportional limit of 117 MPa, and is the same specimen that exhibited an extremely low modulus value. Such a high proportional limit and low modulus indicates that significant damage was done to the specimen. At this time there is no way to go back and determine what happened to this particular test specimen. It was also a bit surprising that the specimens with fatigue pre-conditioning at 150 MPa did not exhibit higher proportional limit values, as is often observed in other CMCs – many of which will show a decrease in the modulus and increase in the proportional limit (often up to near the applied load level) once subjected to a higher load. However, A500 is extensively micro-cracked from processing, so it is unlikely for more than minimal additional matrix cracking during loading to 150 MPa.

Strain-to-failure values versus test condition are shown in Figure 43. There is a lot of scatter in the amount of strain to failure, so no conclusion or observations can be made. While it does appear that the salt fog-exposed specimens do see some reduction in strain to failure, all but one of the test specimens exhibited at least 0.5% strain to failure. This indicates that, while there was damage occurring in the A500 CMC, the specimens that saw burner rig plus salt fog lost very little toughness.

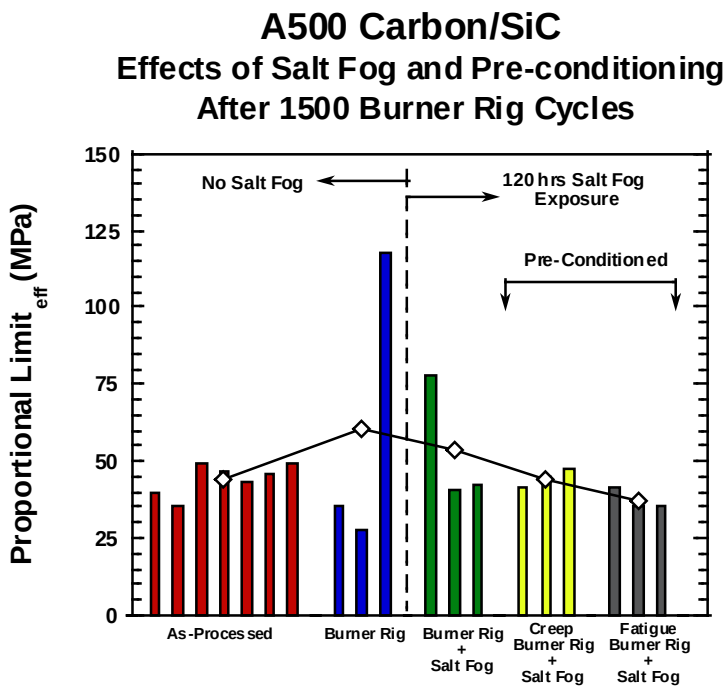

Figure 42. Proportional Limit Versus Test Condition for A500 C/SiC

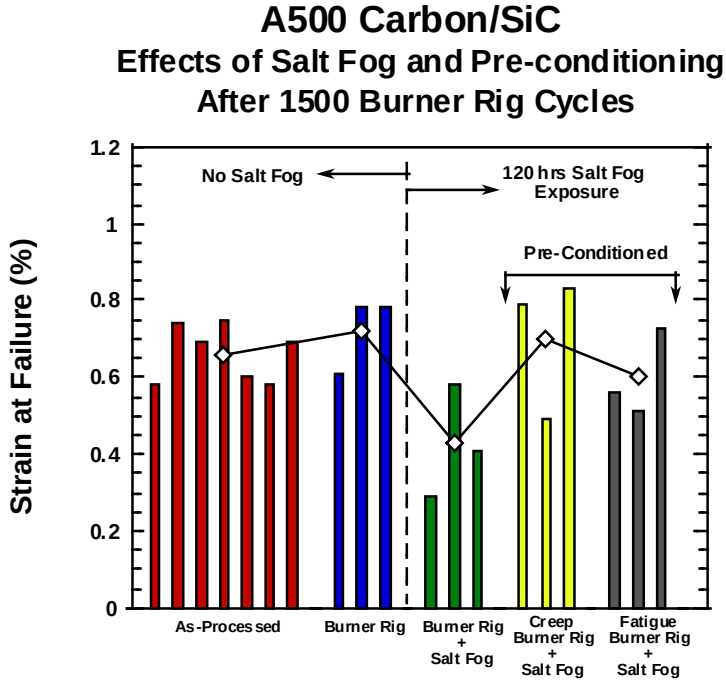

Figure 43. Strain at Failure Versus Test Condition for A500 C/SiC

A representative efficient stress-versus-strain trace for each test condition is shown in Figure 44. In general, all of the tested A500 specimens exhibited typical composite behavior. Each specimen exhibited a very small initial linear region followed by a gradual transition to non-linear behavior with no distinct proportional limit. Strain to failure was 0.5% or greater. As with the bar plots above, the stress-versus-strain traces can be divided into two groups. The as-manufactured and the burn rig traces are very similar, while the three conditions that involved salt fog exposure form a separate group and are very similar. Overall, the A500 CMC exhibited excellent composite behavior for all test conditions.

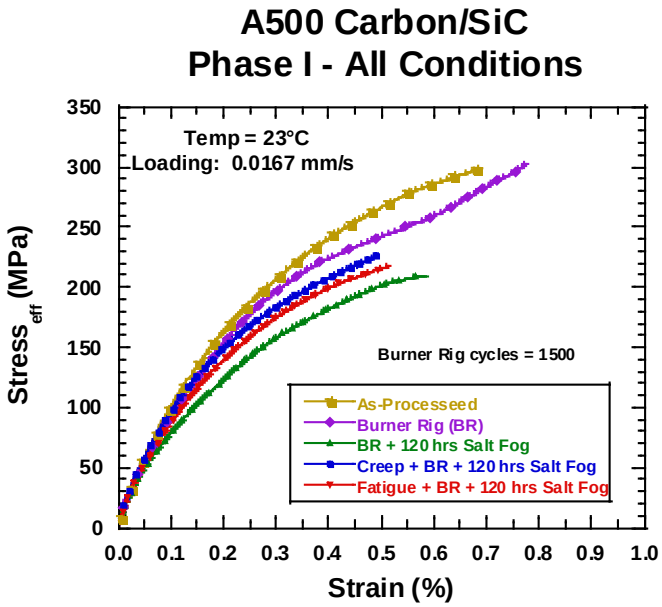

Figure 44. Efficient Stress Versus Strain for As-Manufactured, Burn Rig Tested, and Pre-conditioned A500 C/SiC

Following exposure each test specimen surface condition was documented using optical photograph. Figure 45 shows a failed as-manufactured tensile specimen while Figure 46 is a higher magnification of the surface of the gage section. This serves as a baseline with which to compare the burner rig-exposed specimens.

Figure 47 shows a failed specimen that saw 1500 burner rig cycles and Figure 48 is a higher magnification of the gage section. This sample does exhibit some discoloration in the gage section due to an extremely thin oxide layer forming on the surface of the specimen during exposure to the open flame. The color pattern was dependent on the location with respect to the flame, and indicates that the oxidized layer thickness varies with location and related maximum temperature.

Figure 45. Optical Photograph of A500 C/SiC Tension-Tested As-Manufactured Specimen

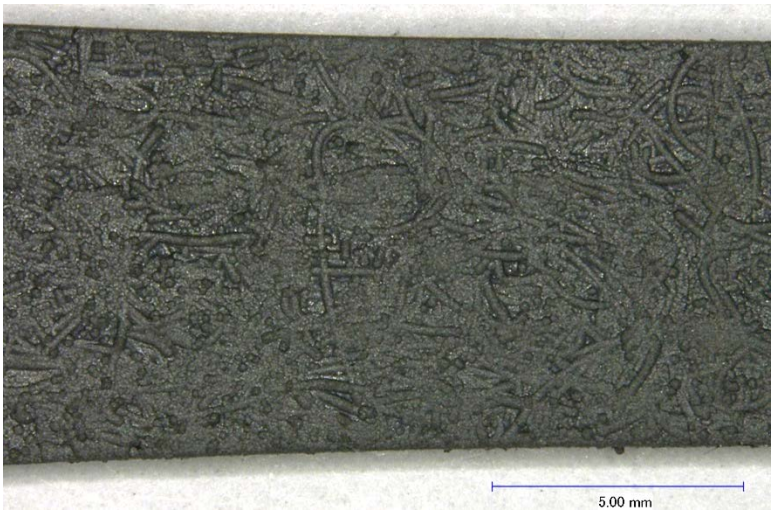

Figure 46. Optical photograph of the Surface Of The Gage Section Of A A500 C/SiC As-Manufactured Test Specimen

Figure 47. Optical Photograph of a A500 C/SiC Tension-Tested Specimen After 1500 Burner Rig Cycles and No Salt Fog Exposure

Figure 48. Optical Photograph Of The Surface Of The Gage Section of A500 C/SiC Specimen After 1500 Burner Rig Cycles and No Salt Fog Exposure

Figure 49 shows an optical photograph of a failed specimen that saw 1500 burner rig cycles plus 120 hours of salt fog exposure, and Figure 50 is a higher magnification of the gage section. As stated in an earlier section, the addition of salt fog exposure resulted in an extensive glassy phase formation in all of the surface cracks, which then flowed onto the surface of the specimens. The same glassy formations were also seen on the surfaces of the pre-conditioned specimens. Figure 51 shows an optical photograph of an A500 C/SiC tension-tested specimen that was fatigue pre-conditioned (1 Hz, 150 MPa, 24ºC, 1000 cycles), followed by 1500 burner rig cycles with 120 hours of salt fog exposure. Figure 52 is a higher magnification of the gage section of this specimen. The surface is identical to the burner rig plus salt fog specimen.

Figure 49. Optical PhotographOf A Tension Tested A500 C/SiC Specimen After 1500 Burner Rig Cycles Plus Salt Fog Exposure

Figure 50. Optical Photograph Of The Surface Of The Gage Section of A500 C/SiC After 1500 Burner Rig Cycles Plus Salt Fog Exposure

Figure 51. Optical Photograph of a A500 C/SiC Tension-Tested Fatigue Specimen Pre-conditioned (1 Hz, 150 MPa, 24ºC, 1000 Cycles) After 1500 Burner Rig Cycles Plus Salt Fog Exposure

Figure 52. Optical Photograph of the Surface of the Gage Section of a A500 C/SiC Fatigue Specimen Pre-conditioned (1 Hz, 150 MPa, 24ºC, 1000 Cycles) After 1500 Burner Rig Cycles Plus Salt Fog Exposure

5.0 DISCUSSION OF TEST RESULTS

In studying the tensile results, there was clear evidence that degradation was occurring in the specimens that saw burner rig plus salt fog exposure. Tensile properties were observed to decrease with increasing cycles. Therefore, it was decided to cut, mount, and polish material from the gage section of tested specimens to study the microstructure of the A500 CMC in detail. Figure 53 and Figure 54 are optical micrographs of a cross-section from an as-manufactured specimen that was tension tested. In the micrographs one can clearly see the multiple layers that make up the sequential matrix. There are periodic cracks in the thicker surface matrix layer, but the individual layers act to deflect the cracks and cause extensive crack bifurcation. Such crack branching results in cracks that have relatively small crack mouth opening displacements (CMODs. It is the tortuous crack pattern and small CMOD that limits the amount of oxygen that can reach the interior of the CMC. In addition, since the cracks do not open very wide, it is much easier for them to be sealed by glass formation.

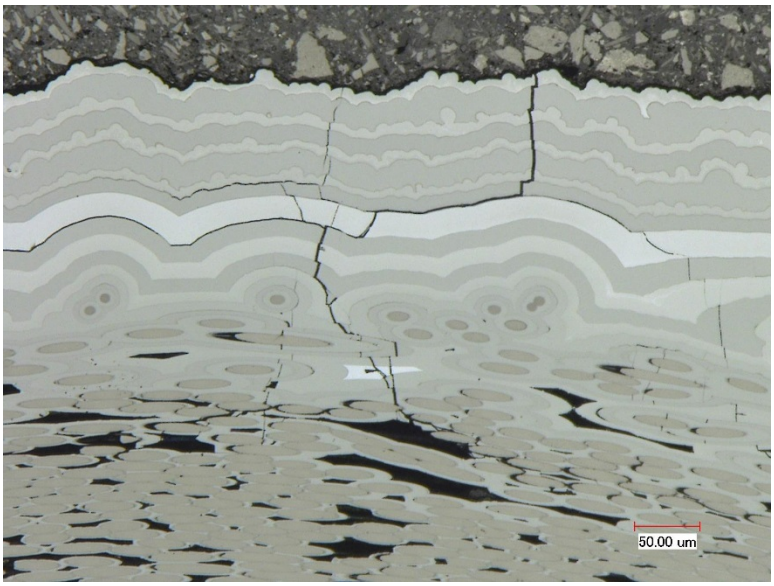

Figure 53. Optical Micrograph Of An As-Manufactured Failed Tensile Specimen (#26)

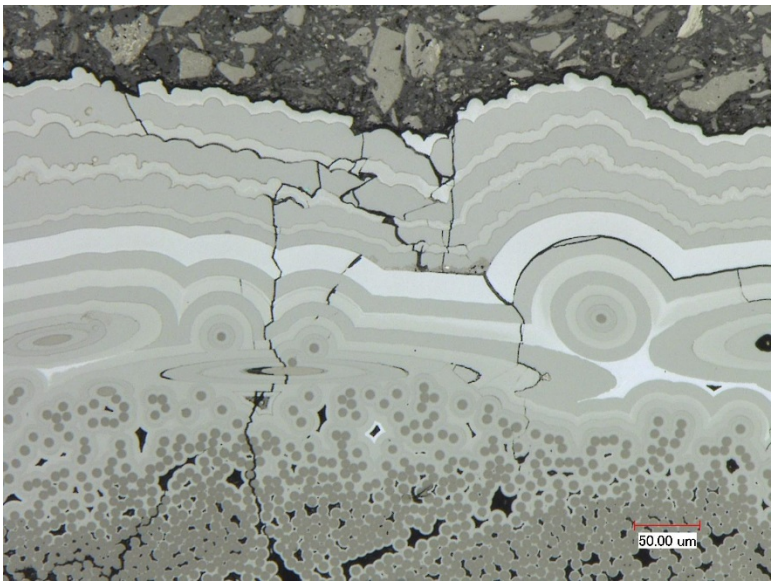

Figure 54. Optical Micrograph Of An As-Manufactured Failed Tensile Specimen (#26)

Figure 55 and Figure 56 are optical micrographs of a specimen that saw 300 burner rig cycles and one salt fog exposure of 24 hours. The surface shows no evidence of oxidation or consumption of any of the layers that make up the sealing phases. The matrix crack is filled with a solid glassy phase which has sealed off the interior of the CMC. This sealing protected the carbon fibers and there is no sign of oxidative attack of the carbon fibers.

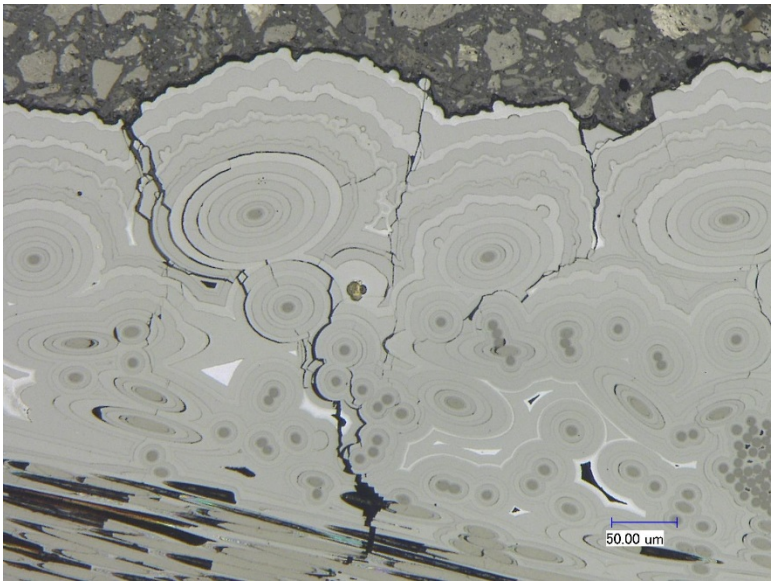

Figure 55. Optical Micrograph Of A Tension-Tested Specimen (#3) After 300 Burner Rig Cycles Plus 24 Hours Salt Fog Exposure

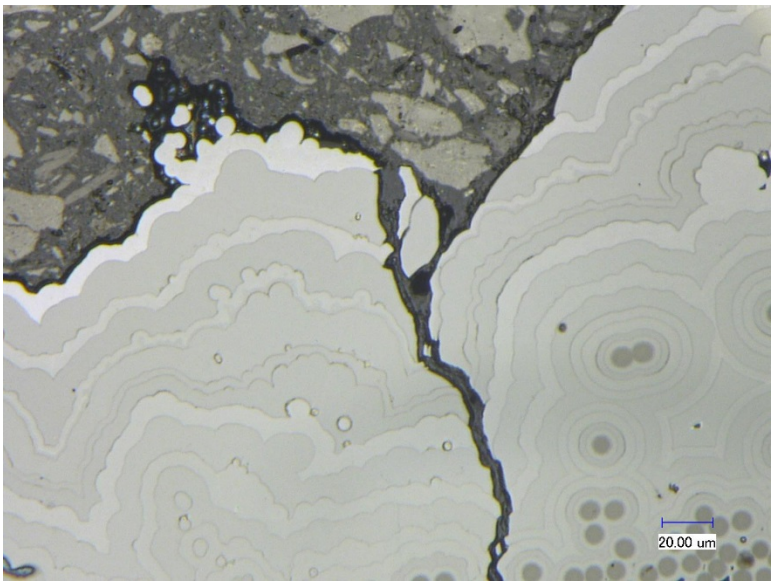

Figure 56. Optical Micrograph Of A Tension-Tested Specimen (#3) After 300 Burner Rig Cycles Plus 24 Hours Salt Fog Exposure

Figure 57 and Figure 58 are optical micrographs for a specimen that saw 600 burner rig cycles plus 48 hours of salt fog exposure. There appears to be some consumption of the individual matrix layers nearest the surface at the location where each matrix crack intersects the surface of the CMC. The consumption is more active for the sealing phases; whereas, the SiC layers are barely affected. A glassy phase has replaced the consumed material and appears to have filled the crack. The first four exterior thick matrix layers (about half the thickness of the seal coat) appear to have been affected. In addition, there appears to be depletion in the first bright white phase layer, but the layer is not consumed. It is important to note that, for this number of cycles, there appears to be no oxidative damage to the carbon fibers, and this matches the tensile data that showed no loss in strength.

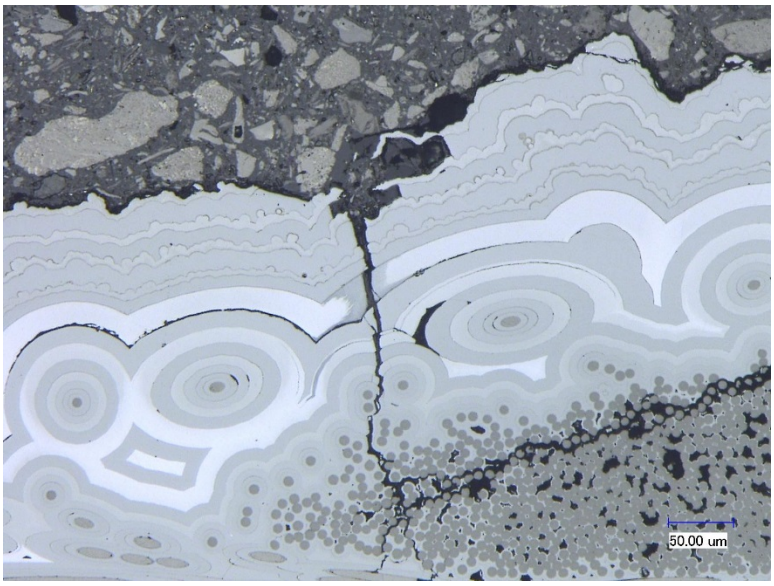

Figure 57. Optical Micrograph Of A Tension-Tested Specimen (#33) After 600 Burner Rig Cycles Plus 48 Hours Salt Fog Exposure

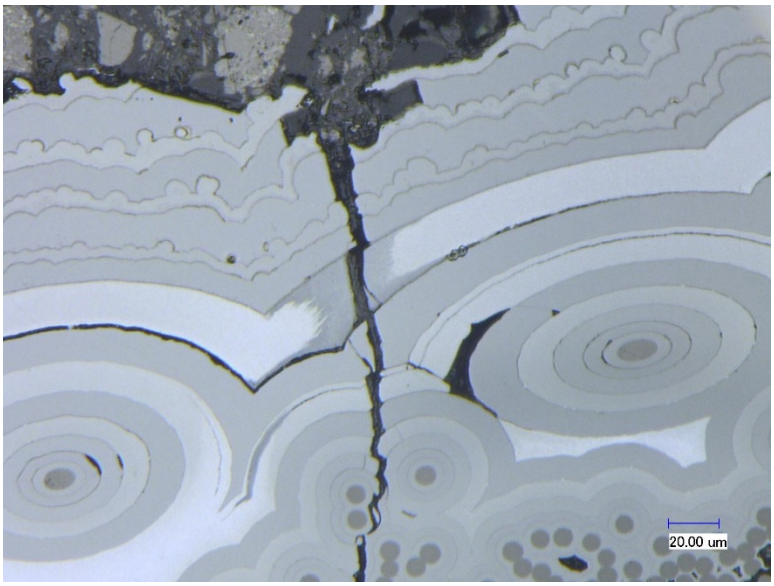

Figure 58. Optical Micrograph Of A Tension-Tested Specimen (#33) After 600 Burner Rig Cycles Plus 48 Hours Salt Fog Exposure

Figure 59, Figure 60, and Figure 61 are optical micrographs of a failed tensile specimen that saw 900 burner rig cycles and 72 hours of salt fog exposure showing that more layers have reacted. The top four layers have been extensively reacted and consumed, with glass formed in their place. The reacted area has significantly widened compared to the specimen that saw 600 burner rig cycles. The crack opening that exposed the seal coat has significantly widened, but has not penetrated into the interior CMC. Some fiber erosion appears to be the start of fiber oxidation at the surface tows in the largest cracks, though the damage to the carbon fibers appears to be

limited. This initial fiber damage likely accounts for the initial 5% drop-off in retained tensile strength measured for these specimens.

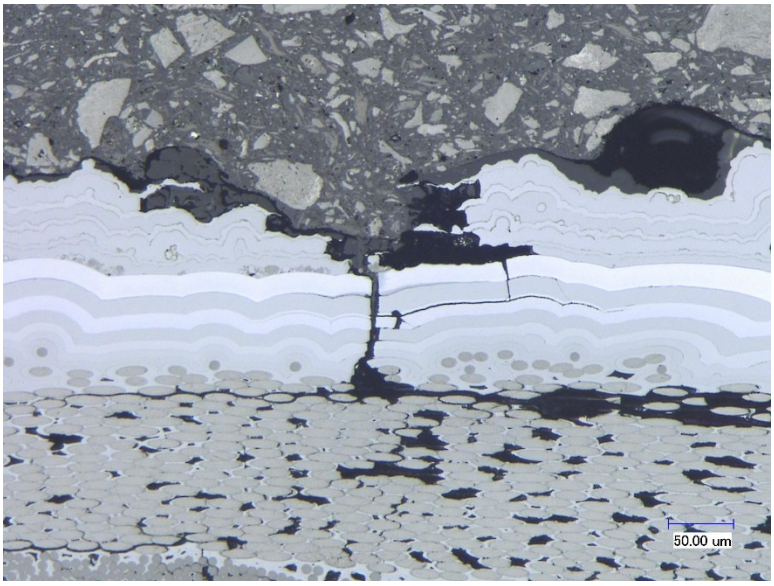

Figure 59. Optical Micrograph Of A Tension-Tested Specimen (#4) After 900 Burner Rig Cycles Plus 72 Hours Salt Fog Exposure

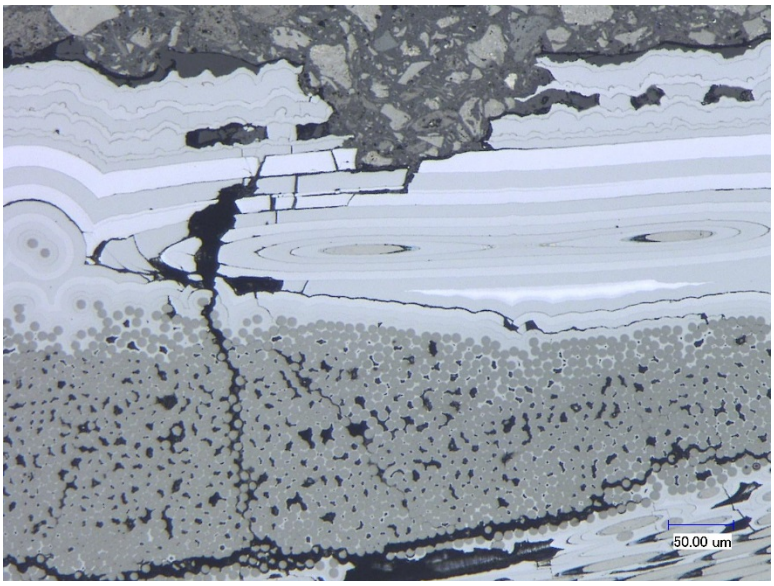

Figure 60. Optical Micrograph Of A Tension-Tested Specimen (#4) After 900 Burner Rig Cycles Plus 72 Hours Salt Fog Exposure

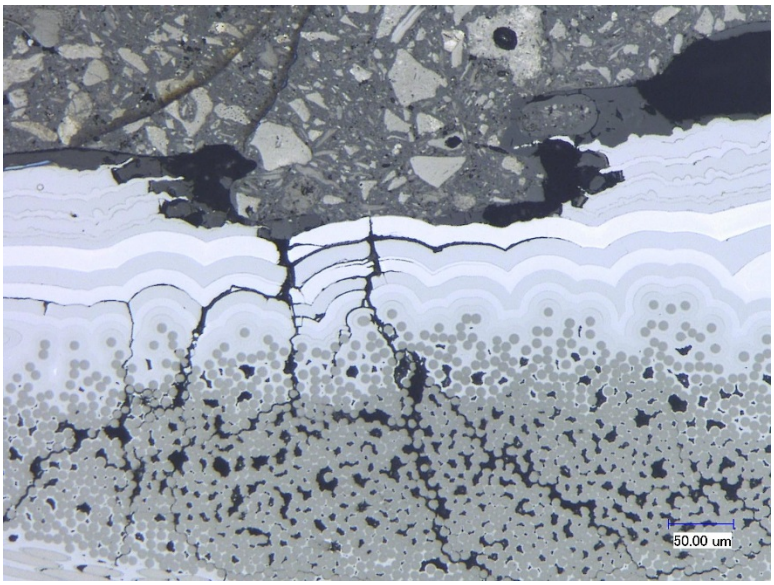

Figure 61. Optical Micrograph Of A Tension-Tested Specimen (#4) After 900 Burner Rig Cycles Plus 72 Hours Salt Fog Exposure

Figure 62 is an optical micrograph of a failed test specimen that saw 1200 burner rig cycles and 96 hours of salt fog exposure. At this number of cycles, there is significantly more material consumed in the first four layers, and the area being consumed has widened to a width of approximately 30-40 fiber diameters. The reactions have now formed a sizable hole in the surface layers, significantly widened the cracks that penetrate from the surface into the interior of the composite, and the oxidation has penetrated into the interior of the composite. There are areas where the entire surface layers have been consumed and replaced with glass. The glassy phase itself also appears to be reacting and becoming more porous, as well as being partially consumed in the crack. It appears the porous glass has essentially flowed and now covers the surface of the CMC on both sides of the crack. In multiple locations, the surface has been breached and significant attack has occurred to the carbon-fiber tows beneath these cracks. It is this attack of the carbon fibers that results in the 11% decrease in strength measured for these specimens.

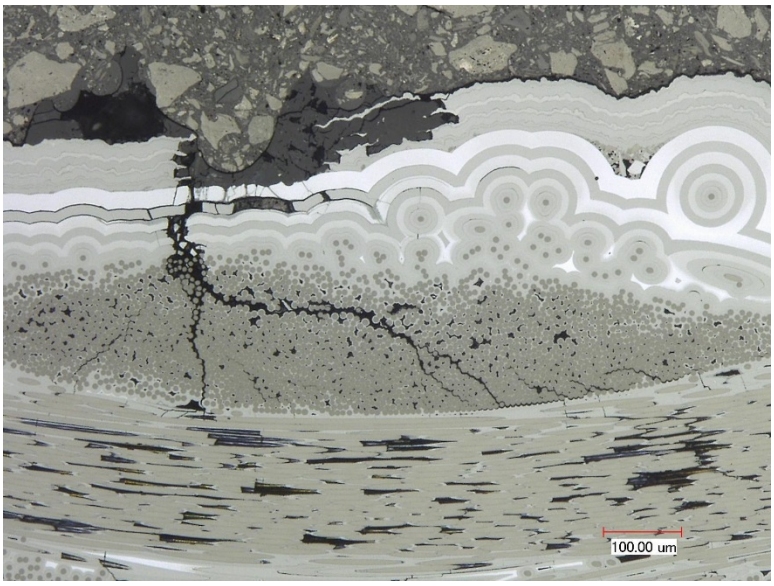

Figure 62. Optical Micrograph Of A Tension-Tested Specimen (#16) After 1200 Burner Rig Cycles Plus 96 Hours of Salt Fog Exposure

Figure 63, Figure 64, Figure 65, Figure 66, and Figure 67 are all optical micrographs of a failed test specimen that saw 1500 burner rig cycles and 120 hours of salt fog exposure. At this cycle count, the locations where there were surface cracks have now resulted in very wide areas where the surface layers have been consumed. The cracks that penetrated from the surface into the interior of the CMC are now significantly wider and no longer appear to be sealed with a glassy phase. There also appears to be oxidation in the first two fiber tows (with significant oxidative attack in the first tow). This attack appears to be consuming entire groups of carbon fibers in the fiber tows, although the SiC matrix is still providing protection within the interior of the specimen. It is important to note that there is not nearly as much glass formation in the matrix cracks and where the matrix use to be. This implies the sealing phases have been converted into a glassy phase, and that the extended cycling and salt fog exposure has resulted in the consumption of the glass. From the micrographs of the surface of these specimens shown earlier, there is extensive foamy glass on the surface of the composite that, at one time, was a solid glassy phase sealing the cracks in the matrix. In Figure 66, faster consumption of the sealing phases in the matrix can be seen, as well as a significant amount of glass that has flowed and is now on the surface of the composite (similar to that seen on the surface of the tested tensile specimens). After exposure to this number of cycles, a significant amount of the solid glassy phase has been removed, allowing for accelerated degradation of the carbon fibers. It is the loss of the sealing phase that results in a reduction of tensile strength of 29% for these specimens.

From studying the micrographs, it is clear that the sealing phases are effective in protecting the A500 CMC up to around 900 burner rig cycles and 72 hours of salt fog exposure. However, it is by 1200 cycles, that the solid glass phase first starts to react, creating a foamy glass and starts to recess. After 1200 cycles, the sealing phases are essentially exhausted and degradation of the carbon fibers accelerates.

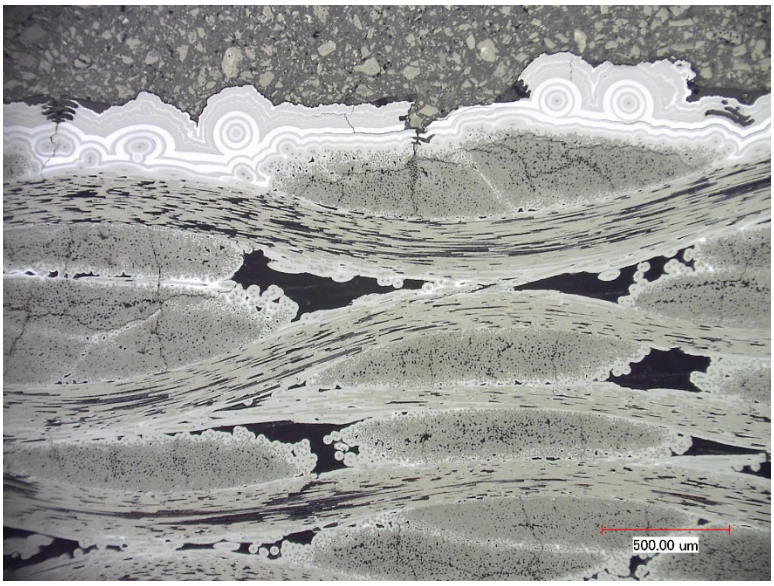

Figure 63. Optical Micrograph Of A Tensile Tested Specimen (#8) After 1500 Burner Rig Cycles and 120 Hours Salt Fog Exposure

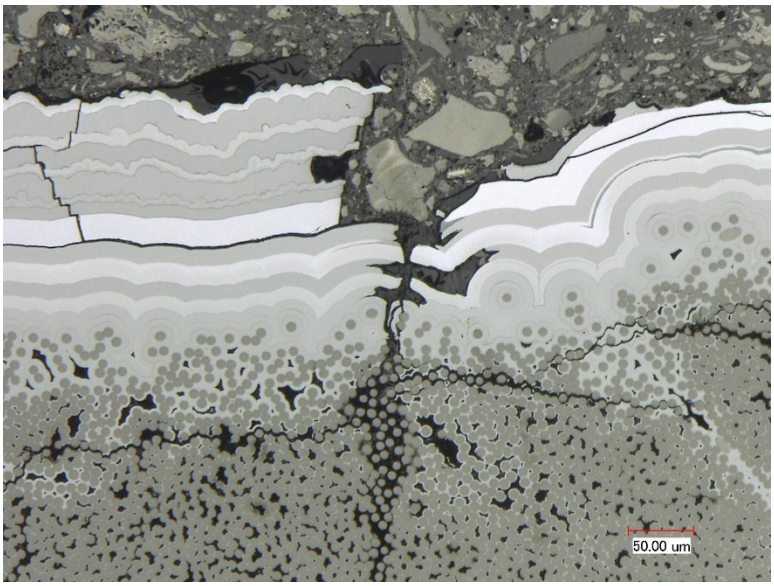

Figure 64. Optical Micrograph Of A Tensile Tested Specimen (#8) After 1500 Burner Rig Cycles and 120 Hours Salt Fog Exposure

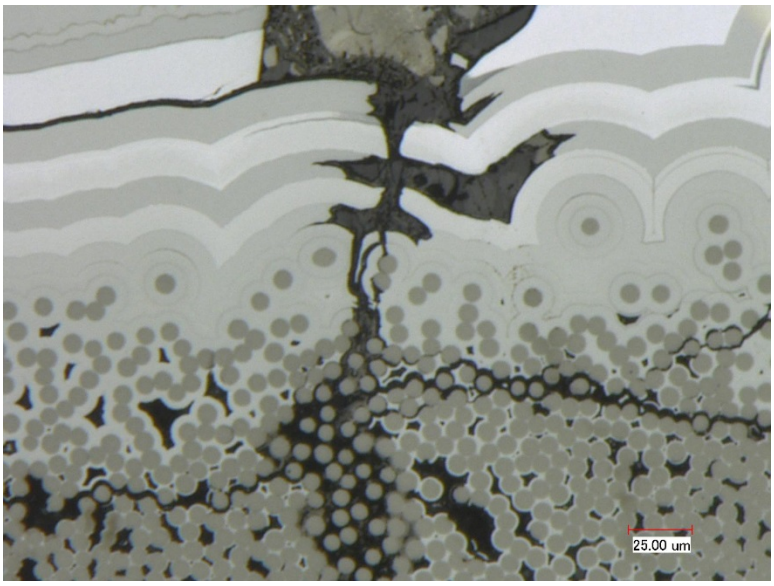

Figure 65. Optical Micrograph Of A Tensile Tested Specimen (#8) After 1500 Burner Rig Cycles and 120 Hours Salt Fog Exposure

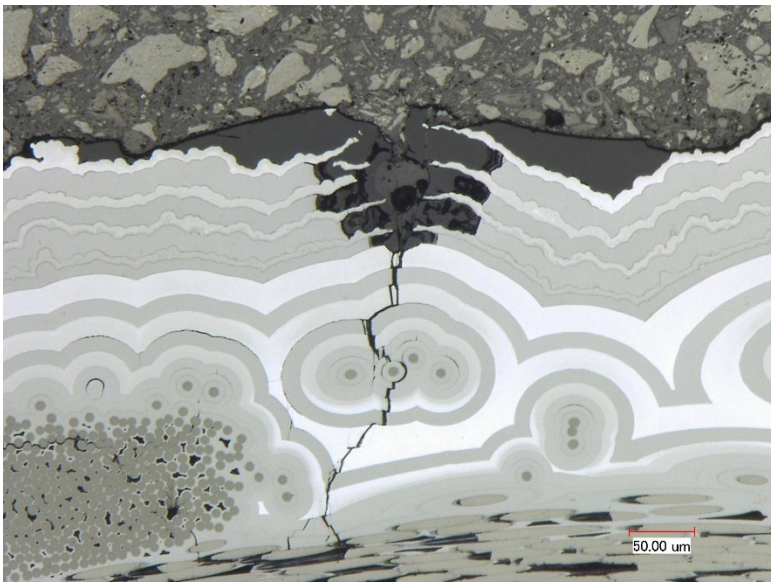

Figure 66. Optical Micrograph Of A Tensile Tested Specimen (#8) After 1500 Burner Rig Cycles and 120 Hours Salt Fog Exposure

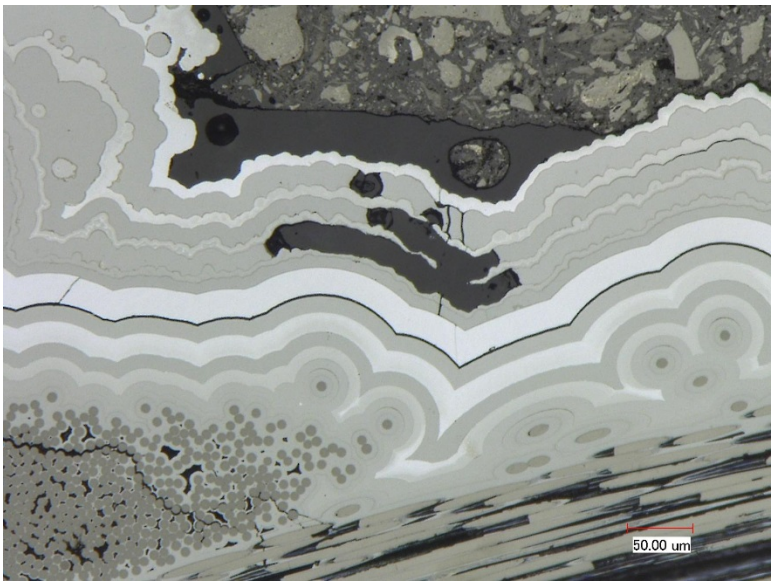

Figure 67. Optical Micrograph Of A Tensile Tested Specimen (#8) After 1500 Burner Rig Cycles and 120 Hours of Salt Fog Exposure

In order to fully understand the degradation, one of the failed burner rig specimens that had seen 1500 cycles with no salt fog was also sectioned and polished to study the microstructure. Figure 68 and Figure 69 are polished cross-sections from that specimen where there has been some modest consumption of the first two or three layers of the matrix, with some layers being consumed faster than others. However, the consumed area is only about 4-6 fiber diameters wide and there is no evidence of any oxidation of the carbon fibers. It appears that reactions are occurring, and matrix is being consumed and replaced with glass, but are much slower and appear similar to the specimens tested between 300 and 600 burner rig cycles with salt fog. Thus, without salt fog, this A500 CMC would exhibit excellent life in an afterburner environment.

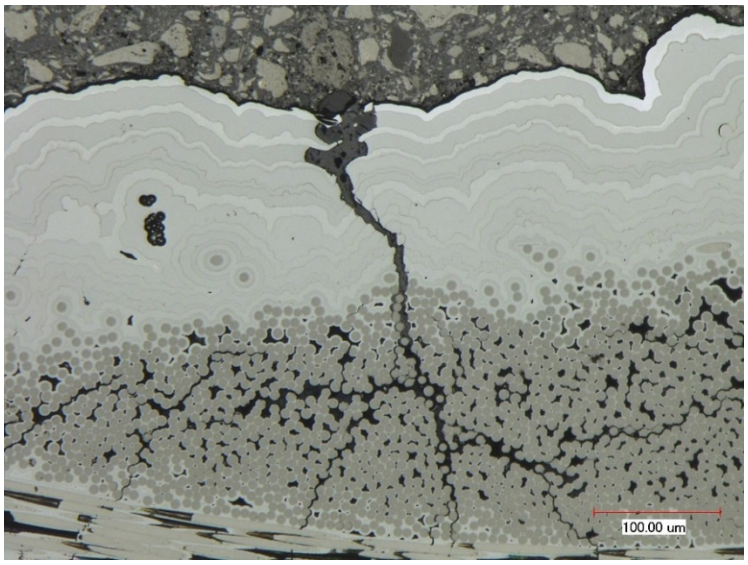

Figure 68. Optical Micrograph Of A Tensile Tested Specimen (#11) After 1500 Burner Rig Cycles and No Salt Fog Exposure

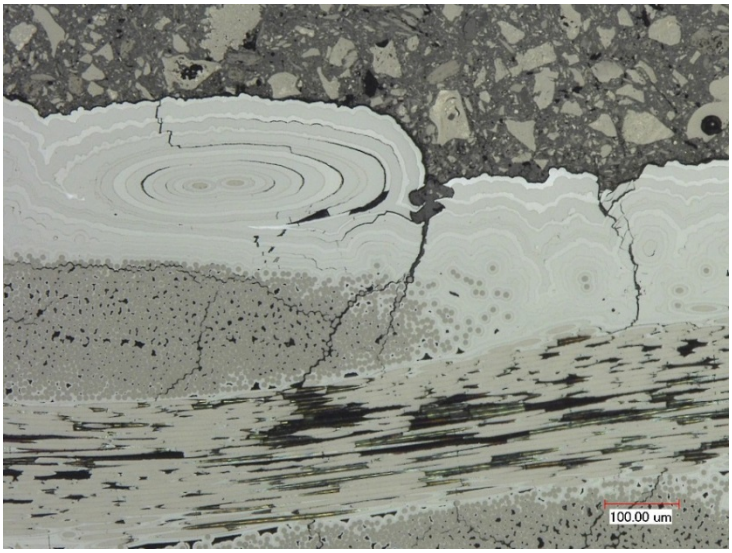

Figure 69. Optical Micrograph Of A Tensile Tested Specimen (#11) After 1500 Burner Rig Cycles and No Salt Fog Exposure

Polished cross-sections of the specimens that saw 1500 burner rig cycles plus 120 hours of salt fog revealed that a substantial amount of the solid glassy phase appears to have been removed from the cracks where it had formed. The appearance on the surface is of a foamy-looking glassy phase. Figure 70 compares the surface of each of the different cycles conducted for burner rig plus salt fog. In this grouping, it can be seen that the glassy phase has significantly started to form by 900 cycles, and continues to expand at 1200 and 1500 burner rig cycles. Figure 71 is a higher resolution optical micrograph of Figure 66 shown earlier. In this figure, the glass can be seen to have filled in the initial matrix crack, and that the sealing phases have been preferentially consumed, while the harder and more stable SiC phase was much slower in being consumed. The production of glass results in a tunneling effect in the softer sealing phases,

while the harder SiC phase is not as rapidly reacted. It can also be seen that only the first four softer layers reacted and, for this crack, the reaction did not reach completely into the first fiber tow. In addition, there is an extensive amount of glassy phase that is now on the surface of the composite, just as observed in Figure 70.

Figure 72 is a low-magnification photograph of a failed tensile specimen that saw 1500 burner rig cycles and a total of 120 hours of salt fog exposure. In observing the fracture surface, there is still good fiber pullout characteristic of good CMC behavior. However, on the surface of the specimen, there is extensive glass formation adjacent to any matrix cracks. As previously stated, the glassy phase on the surface is very foamy and bubbly in nature and, in certain locations, vent holes appear to have formed from a gaseous species caused during the evolution and flow of the glassy phase.

Figure 73, Figure 74, and Figure 75 are higher resolution optical photographs of the surfaces of the specimen shown in Figure 72. These three figures show extensive foamy glassy formation on the surface of the composite. It appears that, after this amount of exposure, the solid glassy phase that originally forms and seals the matrix cracks reacts further, becomes foamy in nature, and deposits on the surface of the test specimens as a foamy white phase. The figures show that, again, extensive gas has been generated, forming bubbles and what appear to be outgassing vent holes.

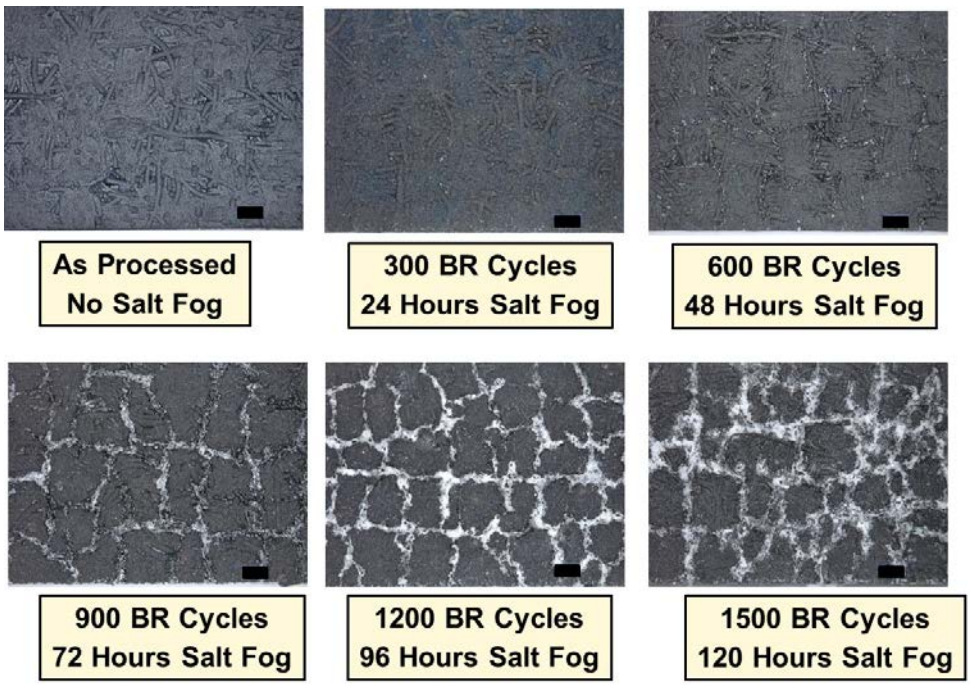

Figure 70. Comparison of Glass Formation on Specimens After Various Numbers of Salt Fog Plus Burner Rig Cycles

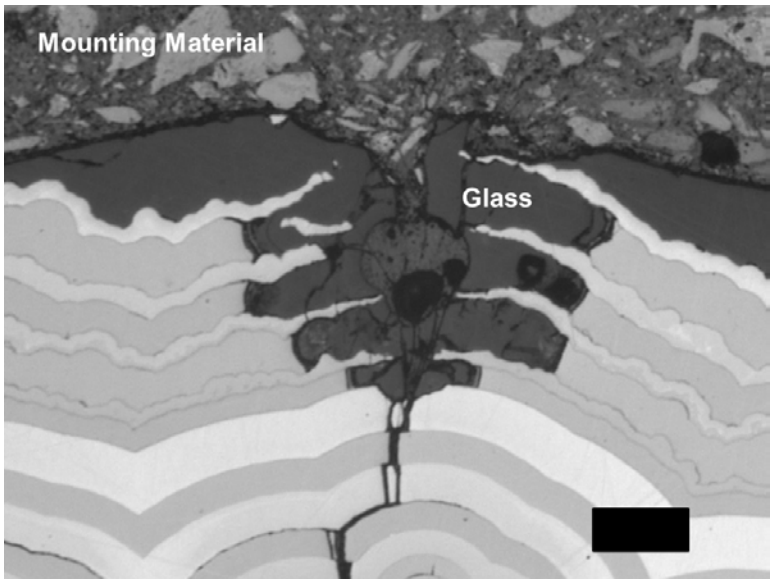

Figure 71. Optical Micrograph Of A Tensile Tested Specimen (#8) After 1500 Burner Rig Cycles and 120 Hours Salt Fog Exposure

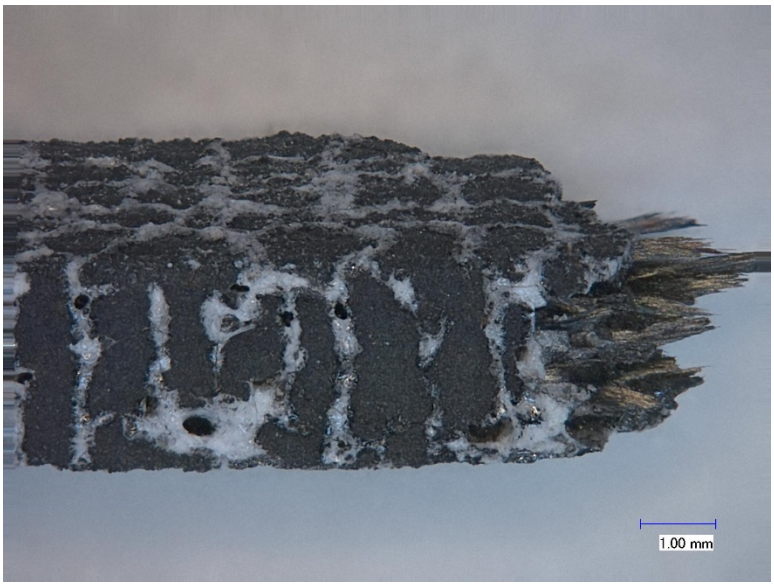

Figure 72. Optical Photograph Of The Surface of Specimen After 1500 Burner Rig Cycles Plus 120 Hours Salt Fog Exposure Showing Significant Glass Formation

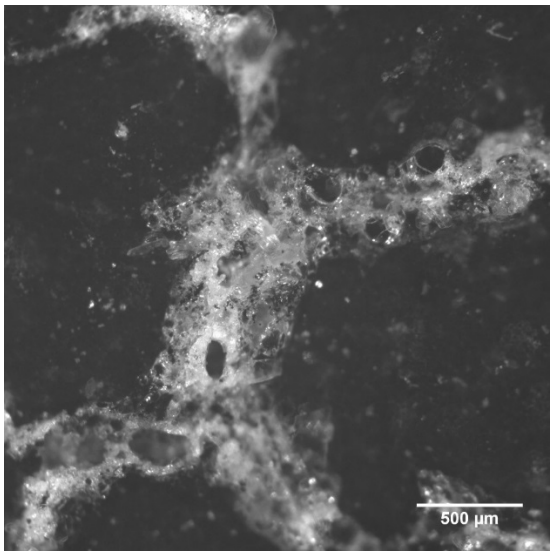

Figure 73. Optical Photograph Of The Surface of Specimen After 1500 Burner Rig Cycles Plus 120 Hours Salt Fog Exposure Showing Glass Formation

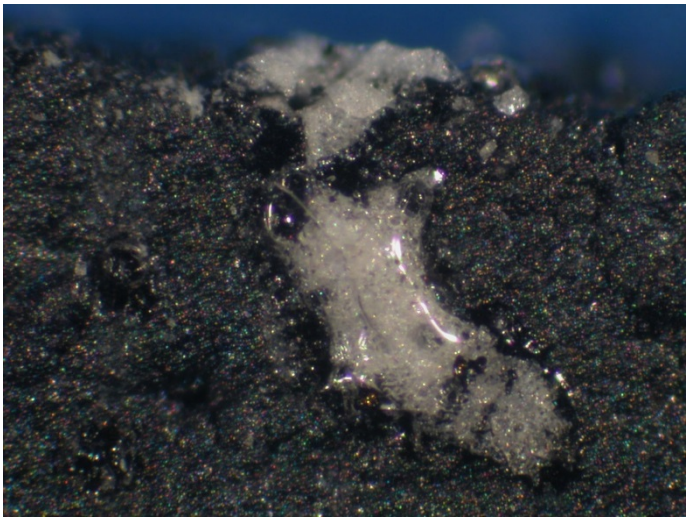

Figure 74. Optical Photograph Of The Surface of Specimen After 1500 Burner Rig Cycles Plus 120 Hours Salt Fog Showing Glass Formation

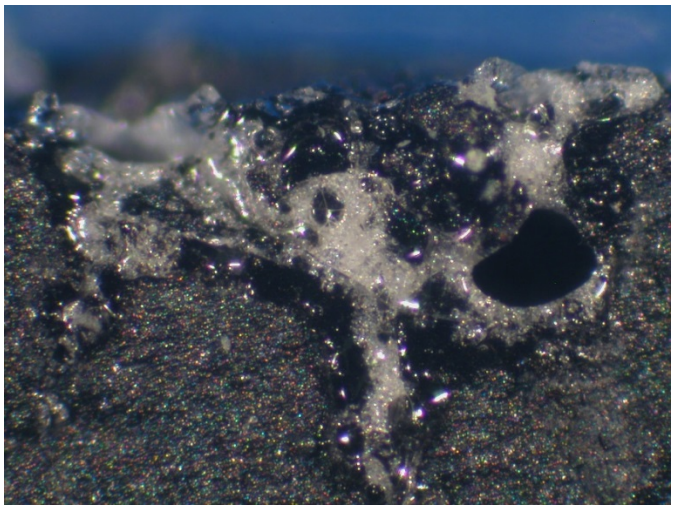

Figure 75. Optical Photograph Of The Surface of Specimen After 1500 Burner Rig Cycles Plus 120 Hours Salt Fog Showing Glass Formation

The USN has previously conducted identical tests in the NAVAIR burner rig with and without salt fog on two other CMCs.

The results for a Nextel 720 fiber-reinforced alumino-silicate are shown in Figure 76 [14]. This CMC does not lose any strength from burner rig cycling alone, but there is significant strength loss (on the order of 55%) from burner rig plus salt fog.

Results for a silicon fiber (Nicalon)-reinforced carbon matrix (SiC/C) CMC that uses a SiC exterior seal coat are shown in Figure 77 [15]. This is the CMC currently flying on the F414 engine that powers the F-18 Super Hornet. From the data in the figure, no loss in strength is seen for burner rig exposure only – in fact, the retained strength actually increases. However, the burner rig plus salt fog does result in a modest 10% drop in strength. These results show why this CMC was selected for the nozzle application. What is important to keep in mind is that, over time, the exterior SiC seal coating spalls off, and then there is very rapid degradation of the CMC. The results of those experiments are compared to those from this study in Figure 78, where it is clear that the A500 CMC exhibits significantly higher strength than the other two CMCs over the entire number of burner rig cycles and salt fog exposures. In addition, A500 C/SiC does not use an exterior seal coat, alleviating any concerns about any coating spallation.

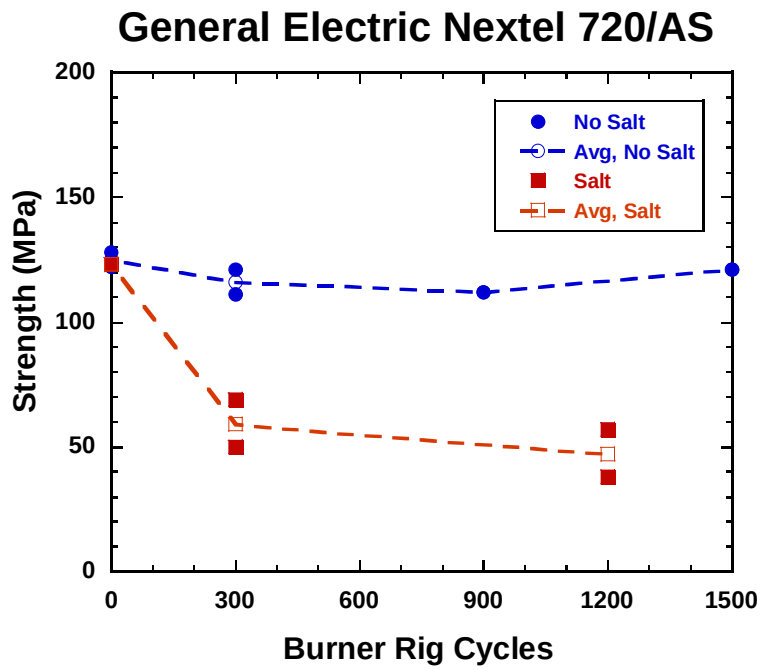

Figure 76. Retained Tensile Strength Versus Number of Burner Rig Cycles for N720/AS With and Without Salt Fog Exposure

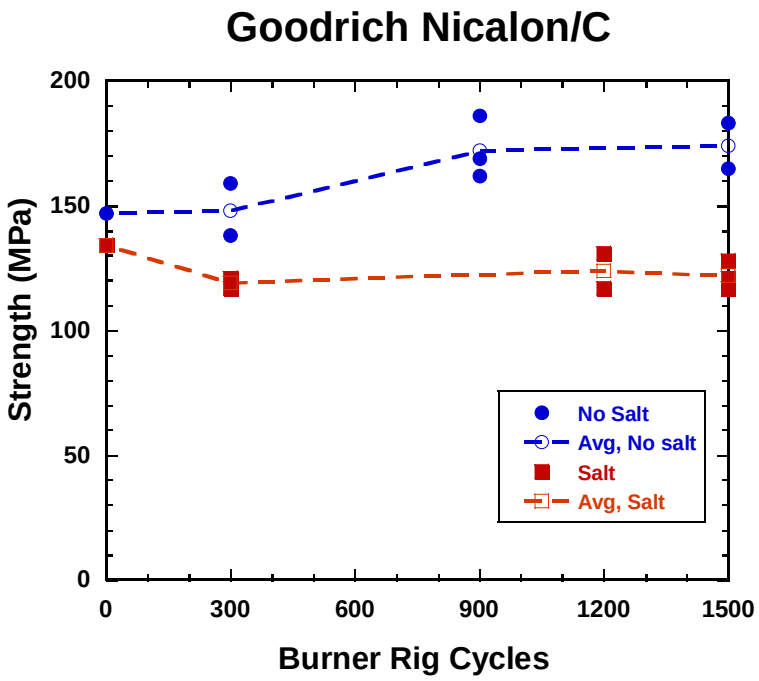

Figure 77. Retained Tensile Strength Versus Number of Burner Rig Cycles for Nicalon/C With and Without Salt Fog Exposure

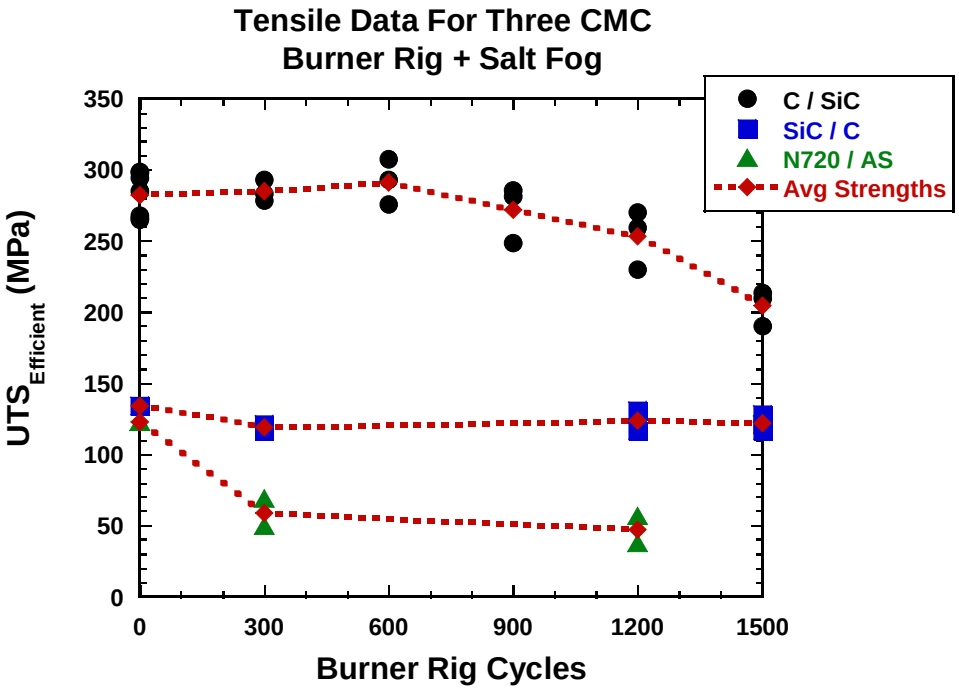

Figure 78. Tensile Results of Burner Rig Plus Salt Fog Exposure for Three Different CMCs

6.0 CONCLUSIONS

Acceptance testing by SPS and the USAF demonstrated that the test specimens made for this study were of excellent quality and exceeded the average value from the database for A500.

The results show that the approach taken to sequence the matrix and adding sealing layers in the A500 material is effective in protecting the carbon fibers under the very aggressive test conditions studied in this investigation. Only at the 1500 cycle count did the material exhibit a significant (29%) debit in retained tensile strength. However, the retained strength is still significantly higher than for Nextel 720/AS and SiC/C CMCs. Other C/SiC CMCs have not performed nearly as well when tested at intermediate temperatures or severe environments [16].

All of the results show that this material still exhibits typical composite behavior after all of the different exposures conducted under this effort. An important observation is that specimens tested with burner rig exposure only (no salt fog) had an average efficient UTS of approximately 295 MPa (higher than the average from the A500 property database) and exhibited a typical-looking composite stress-strain curve. This indicates that the approach taken to use sequential layers in the matrix works well to protect the carbon fibers, even when there are extensive cracks in the matrix. Therefore, in a burner rig environment without severe salt fog exposure, this CMC would exhibit very long lifetimes in service.

Detailed microscopy documented the progression of damage as a function of burner rig plus salt fog cycles. The softer sealing phases begin to react significantly by 900 cycles and are preferentially consumed compared to the much harder SiC phase. This results in a widening of the crack near the surface of the composite that becomes filled in with a solid-looking glassy phase. However, by 1200 cycles, this solid glassy phase formed in the wake of the reacted sealing phases reacts further and becomes foamy in nature. This foamy glass phase no longer seals the cracks and much of it flows out of the crack and deposits on the surface of the composite adjacent to the matrix cracks. This process continues and, at 1500 burner rig cycles and 120 hours of salt fog exposure, the sealing phases are essentially exhausted. Oxidation of the carbon fibers then occurs, resulting in a 29% loss in tensile strength.

The testing performed to date indicates that exposure in a burner rig without and with salt fog did not cause the A500 C/SiC CMC to lose strain capability and become brittle. The residual testing showed that the material still exhibits composite behavior and good strain to failure.

The salt fog exposure coupled with the burner rig testing to 1500 cycles had a measureable degrading effect on the durability of the material, decreasing tensile strength by 29%. It does not appear that the pre-conditioning, either by creep or fatigue, had any additional degrading effects. This indicates that any additional matrix cracks that may have formed during the pre-conditioning were all sealed the same as those formed during the manufacturing process. At the same time, the salt fog is aggressive enough to begin to overcome the material's glassy sealing mechanisms after approximately 1200 burner rig cycles.

7.0 RECOMMENDATIONS

The material has performed well under these very aggressive test conditions. The CMC exhibits post-exposure composite behavior and good retained strength. The results from this investigation indicate that the A500 CMC should perform well in an aerospace turbine engine exhaust nozzle environment.

8.0 REFERENCES

[1] Ojard, G., Naik, R., Cairo, R., Hornick, J., Linsey, G., Brennan, J. and Amos, J., "Mechanical Characterization of Ceramic Matrix Composite Components", Structural Integrity for the Next Millennium; Proceedings of the 20th Symposium of the Internal Committee on Aeronautical Fatigue, 14-16 July 1999, Bellevue, WA, 1999, Vol. II, pp. 1151-1167.

[2] Chawla, K.K., Ceramic Matrix Composites, Chapman and Hall, New York, 1993.

[3] Chawla, K.K., Composite Materials, 2nd Edition, Springer, New York, 2001.

[4] Zawada, L., Richardson, G., and Spriet, P., "Ceramic Matrix Composites for Aerospace Turbine Engine Exhaust Nozzles," in High Temperature Ceramic-Matrix Composites V, edited by Mrityunjay Singh, Ronald J. Kerans, Edgar Lara-Curzio, and Roger Naslain, September 2004, pp. 491-498.

[5] Kestler, R. and Purdy, M., "SiC_{f}/C for Aircraft Exhaust" presented at ASM International's 14th Advanced Aerosapce Materials and Processes Conference, Dayton, Ohio, June 9-13, 2003 (unpublished).

[6] Staehler, J.M. and Zawada, L.P., "Performance of Four Ceramic-Matrix Composite Divergent Flap Inserts Following Ground Testing on an F110 Turbofan Engine", *J. Am. Ceram. Soc.,* 83 [7] 1727-38 (2000)

[7] Razzell, A.G., "Rolls-Royce Experience in Ceramic Matrix Composite Demonstration", in Ceramic Gas Turbine Engine Design and Test Experience, Eds. van Roode, M., Ferber, M.K. and Richerson, D.W., ASME Press, Chapter 26, 2002

[8] Farizy, G., Cher Mant, J.L., Sangleboeuf, J.C., and Vicens, J., "SiCf–SiBC composites: microstructural investigations of the as-received material and creep tested composites under an oxidative environment," *Journal of Microscopy,* Vol. 210, Pt. 2, May 2003, pp. 176-186.

[9] Bouillon, F. Abbé, S. Goujard, E. Pestourie, and G. Habarou, "Mechanical and thermal properties of a self-sealing matrix composite and determination of the life time duration", 24th Annual Conference on Composites, Advanced Ceramics, Materials, and Structures, Volume 21, Issue 3, 2000, p. 459.

[10] Viricelle, J.P., Goursat, P., and Bahloul-Hourlierd, X., "Oxidation behavior of a multi-layered ceramic-matrix composite (SiC)f/C/(SiBC)," *Composite Science and Technology,* 61, 607–614. (2001)

[11] Bouillon, E.P., Lamouroux, F., Baroumes, L., Cavalier, J.C., Spriet, P.C., and Habarou, G., "An Improved Long Life Duration CMC for Jet Aircraft Engine Applications", ASME paper No. GT-2002-30625, 2002.

[12] Bouillon, E.P., Abbé, F., Goujard, S., Pestourie, E., and Habarou, G., 2000, "Mechanical and Thermal Properties of a Self-Sealing Matrix Composite and Determination of the Life Time Duration", Ceram. Eng. and Sci. Proc., 21(3), pp. 459-467.

[13] Bouillon, E.P., Ojard, G.C., Habarou, G., Spriet, P.C., Lecordix, J.L., Feindel, D.T., Linsey, G.D., and Stetson, D.P., "Characterization and Nozzle Test Experience of a Self Sealing Ceramic Matrix Composite for Gas Turbine Applications", ASME Turbo Expo 2002, Amsterdam, Netherlands, June 3-7, 2002, ASME Paper 96-GT-284.

[14] Richardson, G.Y, Lei, C.S., and Singh, R.N., "Influence of Turbine Engine Environment on the Mechanical Properties of Ceramic Matrix Composites," 34th International SAMPE Technical Conference Proceedings, November 4-7, 2002, Baltimore, MD.

[15] Richardson, G.Y., Lei, C.S., and Singh, R.N., Mechanical Properties of Ceramic Matrix Composites Exposed to Rig Tests," 28th International Conference on Advanced Ceramics and Composites, 2004, American Ceramic Society, Westerville, Ohio.
[16] Verrilli, M., Kantzos, P., and Telesman, J., "Characterization of Damage Accumulation in a Carbon Fiber-Reinforced Silicon Carbide Ceramic Matrix Composite (C/SiC) Subjected to Mechanical Loadings at Intermediate Temperature", ASTM STP 1392, Mechanical, Thermal and Environmental Testing and Performance of Ceramic Composites and Components, M.G. Jenkins, E. Lara-Curzio and S.T. Gonczy, eds., American Society for Testing and Materials, West Conshohocken, PA, pp. 245-261, 2000.

LIST OF SYMBOLS, ABBREVIATIONS, AND ACRONYMS

AFRL	Air Force Research Laboratory
AFRL/RXCC	Composites Branch, Structural Materials Division of the Materials & Manufacturing Directorate, Air Force Research Laboratory
ASTM	American Society for Testing and Materials
B	Boron
C	Carbon
CMC	Ceramic matrix composite
C/SiC	Carbon fiber-reinforced silicon carbide
CMOD	Crack mouth opening displacement
CTE	Coefficient of thermal expansion
CVI	Chemical vapor infiltration
DTIC	Defense Technical Information Center
EAR	Export Administration Regulation
EBC	Environmental barrier coating
Ei	Modulus per individual cycle
Eo	Initial modulus
ITAR	International Traffic in Arms Regulation
MATE	Material Analysis and Testing
MI	Melt infiltration
MTS	Material Systems Inc.
NAVAIR	Naval Air Systems Command
PIP	Polymer infiltration and pyrolysis
PL	Proportional Limit
SEM	Scanning Electronic Microscope
Si	Silicon
SiC	Silicon carbide
SPS	Snecma Propulsion Solide
UDRI	University of Dayton Research Institute
USAF	United States Air Force
USN	United States Navy
UTS	Ultimate tensile strength